



HHS Public Access

Author manuscript

Sci Transl Med. Author manuscript; available in PMC 2018 October 13.

Published in final edited form as:

Sci Transl Med. 2018 April 04; 10(435): . doi:10.1126/scitranslmed.aao6975.

EMERGING INFECTIONS:

Postnatal Zika virus infection is associated with persistent abnormalities in brain structure, function, and behavior in infant macaques

Maud Mavigner¹, Jessica Raper², Zsafia Kovacs-Balint², Sanjeev Gumber², Justin T. O'Neal³, Siddhartha K. Bhaumik¹, Xiaodong Zhang², Jakob Habib¹, Cameron Mattingly¹, Circe E. McDonald³, Victoria Avanzato¹, Mark W. Burke⁴, Diogo M. Magnani⁵, Varian K. Bailey⁵, David I. Watkins⁵, Thomas H. Vanderford², Damien Fair⁶, Eric Earl⁶, Eric Feczko⁶, Martin Styner⁷, Sherrie M. Jean², Joyce K. Cohen², Guido Silvestri^{2,8}, R. Paul Johnson², David H. O'Connor⁹, Jens Wrammert¹, Mehul S. Suthar^{1,3}, Mar M. Sanchez^{2,10}, Maria C. Alvarado^{2,10}, and Ann Chahroudi^{1,2,11,*}

¹Department of Pediatrics, Emory University School of Medicine, Atlanta, GA, 30322 USA.

²Yerkes National Primate Research Center, Emory University, Atlanta, GA, 30329 USA.

³Emory Vaccine Center, Atlanta, GA, 30329 USA.

⁴Department of Physiology and Biophysics, Howard University, Washington, DC, 20060 USA.

⁵Department of Pathology, University of Miami, Miami, FL, 33146 USA.

⁶Oregon Health and Science University, Portland, OR, 97239 USA.

⁷Department of Psychiatry, University of North Carolina, Chapel Hill, NC, 27599 USA.

⁸Department of Pathology and Laboratory Medicine, Emory University School of Medicine, Atlanta, GA, 30322 USA.

⁹Wisconsin National Primate Research Center, University of Wisconsin-Madison, Madison, WI, 53715 USA.

¹⁰Department of Psychiatry and Behavioral Sciences, Emory University School of Medicine, Atlanta, GA, 30322 USA.

¹¹Children's Healthcare of Atlanta, Atlanta, GA, 30322 USA.

Abstract

The Zika virus (ZIKV) epidemic is associated with fetal brain lesions and other serious birth defects classified as congenital ZIKV syndrome. Postnatal ZIKV infection in infants and children

*To whom correspondence should be addressed: Ann Chahroudi, achahro@emory.edu.

Author contributions: A.C. designed the study with input from M.M., M.A., M.S.S., J.W., D.H.O., T.H.V., R.P.J., D.I.W. and G.S. M.S.S. provided the virus. J.R. and M.C.A. performed the HI test and interpreted the data. Z.K-B., M.M.S. and X.Z. interpreted the neuroimaging. D.F., E.F., E.E., and M.S. provided tools for imaging analysis. S.G. and M.W.B. performed histopathology. S.K.B. and J.W. performed and analyzed ELISA and neutralization assays. J.T.O., C.E.M., M.S.S., V.K.B., D.M.M., and D.I.W. performed and analyzed data from virologic assays with help from C.M. J.H., C.M., and M.M. processed samples. S.M.J. and J.K.C. provided animal care and collected samples. A.C., M.M., and V.A. wrote the manuscript with help from the other authors.

Competing interests: D.H.O. is a paid a member of the Institutional Biosafety Committee for Takeda Vaccines, that is involved in ZIKV research.

has been reported; however, data on brain anatomy, function, and behavioral outcomes following infection are absent. We show that postnatal ZIKV infection of infant rhesus macaques (RMs) results in persistent structural and functional alterations of the central nervous system compared to age-matched controls. We demonstrate ZIKV lymphoid- and neuro-tropism in infant RMs and histopathologic abnormalities in the peripheral and central nervous systems including inflammatory infiltrates, astrogliosis, and Wallerian degeneration. Structural and resting state functional Magnetic Resonance Imaging (MRI/rs-fMRI) show persistent enlargement of lateral ventricles, maturational changes in specific brain regions, and altered functional connectivity (FC) between brain areas involved in emotional behavior and arousal functions, including weakened amygdala-hippocampal connectivity in two out of two ZIKV-infected infant RMs several months after clearance of ZIKV RNA from peripheral blood. ZIKV infection also results in distinct alterations in the species-typical emotional reactivity to acute stress, which were predicted by the weak amygdala-hippocampal FC. We demonstrate that postnatal ZIKV infection of infants in this model impacts neurodevelopment, suggesting that long-term clinical monitoring of pediatric cases is warranted.

Introduction

Zika virus (ZIKV) is a mosquito-borne flavivirus associated with severe birth defects when women are infected during pregnancy (1-3). ZIKV was first isolated in 1947 from rhesus macaques (RMs) (4), then from humans in 1952 (5), and its passage into the brain and ability to induce pathological changes has been reported since the late 1950s (6-8). Recent outbreaks resulting in congenital defects have caused ZIKV to be considered a global health emergency (9). Congenital infection with ZIKV occurs throughout gestation with resultant microcephaly and other brain malformations in fetuses and newborns (10-13).

Whereas critical steps in the formation of the central nervous system take place *in utero*, postnatal development of the brain is a highly dynamic process. In the first year of life, drastic and rapid changes occur, including doubling of brain volume, increased synapse formation, pruning and myelination (14-17). Limbic regions that regulate behavior, such as the hippocampus, undergo substantial postnatal growth and maturation (18). The prolonged synaptic proliferation and neuronal maturation during the postnatal period and early childhood contributes to social learning and plasticity, but also allows for environmental factors to impact the adult configuration (19). We hypothesized that infection with ZIKV during the first year of life may therefore have adverse neuroanatomic and functional consequences that lead to persistent behavioral abnormalities.

The potential for ZIKV to negatively impact brain development in the first year of life is suggested by other viral infections that can be acquired during infancy, such as Cytomegalovirus (CMV) and Human Immunodeficiency Virus (HIV). These infections are transmitted *in utero* but also postnatally via breastfeeding and can lead to significant long-term neurologic complications, such as encephalopathy and cognitive impairment (20-22). The route of postnatal transmission of ZIKV differs from CMV and HIV (arthropod vs. breast milk). However, we posit that when infection occurs during the critical period of brain growth in infancy, like CMV and HIV, postnatal ZIKV infection may cause sequelae similar

to that observed in congenital infection. In addition, the demonstrated neuro-tropism of ZIKV in both fetuses and adults suggests that a similar pattern of infection and resultant neuronal damage may be seen in infants. Postnatal ZIKV of infants and children is reported (23, 24); however, detailed clinical data regarding the outcome of early postnatal ZIKV infection in humans are lacking. Without these data, the Centers for Disease Control and Prevention currently recommends only routine pediatric follow up for infants and children with postnatal acquisition of ZIKV (25).

We sought to evaluate the long-term impact of postnatal ZIKV infection on infant brain development by performing a longitudinal study in infant RMs infected five weeks after birth. The model of ZIKV infection of adult macaques has been established to recapitulate key features of human infection (26-29). Our evaluation of experimental postnatal ZIKV infection in infant RMs included structural and functional Magnetic Resonance Imaging (MRI) brain scans at three and six months of age as well as testing of socio-emotional behavior at six and twelve months of age. We here report that postnatal ZIKV infection in infant RMs is associated with neuroinvasion, enlargement of lateral ventricles, and specific maturational alterations in the hippocampus and other brain regions. Furthermore, we observed altered functional connectivity (FC) between brain regions regulating emotional behavior and arousal functions (e.g., between amygdala and hippocampus) that were predictive of distinct alterations in the species-typical emotional reactivity to acute stress. Taken together, this work demonstrates the pathologic features of postnatal ZIKV infection in the first year of life.

Results

Postnatal ZIKV infection: viral dynamics and tissue tropism.

Eight infant RMs were examined, six of which were challenged subcutaneously (sc) at a median age of 37.5 days (29-38 days) with 10^5 plaque forming units (pfu) of ZIKV PRVABC59 (33). Two of these ZIKV-infected infants and two age-matched, similarly-reared, uninfected control infants (all females) were followed until twelve months of age. The remaining four ZIKV-infected infant RMs (two females and two males) were euthanized during the first two weeks after infection for tissue analysis (Fig. S1). Clinical and hematological parameters remained stable in infant RMs exposed to ZIKV postnatally (Fig. S2). ZIKV RNA in plasma peaked at day 2-3 post infection (p.i.), with concentrations ranging from 1.7×10^6 to 3×10^7 copies of ZIKV RNA per ml of plasma (Fig. 1A). Consistent with previous reports in adult macaques (28, 29), ZIKV RNA was rapidly cleared from plasma, reaching undetectable concentrations by day 7 p.i. (Fig. 1A). We did not detect ZIKV RNA in saliva or cerebrospinal fluid (CSF) from infant RMs, and ZIKV RNA was quantified in the urine of three infants at very low concentrations (15-37 copies/ml) only at day 2-3 p.i. (Table S1).

To assess ZIKV tissue tropism, two ZIKV-infected infant RMs were euthanized at predicted peak viremia (day 3 p.i.) and two were euthanized following resolution of viremia (day 14-15 p.i.). At days 3 and 14-15 p.i. ZIKV RNA was detected by quantitative RT-PCR at concentrations ranging from 1×10^2 to 6×10^5 copies per microgram of RNA in lymph nodes located in the head, neck, axilla, abdomen, pelvis, as well as in the spleen (Fig. 1B).

Additionally, at day 14-15 p.i., ZIKV RNA was quantified by RT-PCR in several peripheral and central nervous system tissues including cauda equina, trigeminal ganglion, frontal cortex, parietal cortex and occipital cortex (Fig. 1B). ZIKV RNA was also detected *in situ* by RNAscope hybridization in the cauda equina and in the granular cell layer of the cerebellum at day 14-15 p.i. (Fig. 1C). Confocal microscopy analyses of these tissues demonstrated that productively infected ZIKV RNA positive cells were CD68/CD163+ microglial cells in the cauda equina and cerebellum as well as NeuN+ neurons in the granular cell layer of the cerebellum (Fig. S3).

Humoral immune responses to postnatal ZIKV infection.

Postnatal ZIKV infection of infant RMs resulted in the rapid generation of humoral immune responses, with ZIKV Envelope (E)-specific IgM detected in plasma of infant RMs by day 7 p.i., with concentrations declining by day 58 p.i. (Fig. 2A) and ZIKV E-specific IgG detected in infant RMs by day 10 p.i. and persisting for up to 142 days p.i. (Fig. 2B). Using focus reduction neutralization test (30), anti-ZIKV neutralization activity was measured in plasma of ZIKV-infected infant RMs by day 10 p.i. and persisted for up to 142 days p.i. (Fig. 2C). These results suggest that infant RMs mount a similar humoral immune response to ZIKV as described in adult RMs (28).

Neurohistopathology of postnatal ZIKV infection.

Central and peripheral nervous system tissues were further subjected to histopathological analysis and immunohistochemistry to investigate the consequences of ZIKV neuroinvasion in postnatally infected infants as compared to age-matched controls. The entire brain and spinal cord were examined for pathologic lesions, and selected images were captured for further analysis. By day 14 p.i., consistent with ZIKV neuroinvasion, inflammatory infiltrates were observed in the brain and spinal cord of ZIKV-infected RM. A representative image of occipital cortex from a ZIKV-infected infant RM with multifocal meningeal mononuclear cell infiltrates is shown in Fig. 3A. The anterior thoracic spinal cord contained circumscribed inflammatory foci in white matter, with evidence of Wallerian degeneration with multiple dilated axons and spheroid formation (Fig. 3B). Examination of the ependymal epithelial cell lining of the basal ganglia revealed hypercellularity of stromal glial cells that was not present in controls (Fig. 3C). Multifocal perivascular inflammatory cells composed predominately of plasma cells, other lymphocytes, and few macrophages were present in the cauda equina (Fig. 3D). Moreover, glial nodules were observed in white matter of the occipital cortex and grey matter of the basal ganglia (Fig. 4A). Immunohistochemistry confirmed increased density of glial fibrillary acidic protein (GFAP)-positive reactive astrocytes as compared to controls, indicating astrogliosis in these brain regions (Fig. 4B). Caspase-3 staining revealed increased apoptosis in ZIKV-infected infant RMs compared to controls (Fig. 4C). Similar brain lesions including gliosis and axon injuries have been reported in the fetus of a pigtail macaque infected by ZIKV during gestation (26) and in autopsy findings from *in utero* ZIKV-infected human fetuses (2).

Volumetric changes in specific brain areas: structural MRI analyses.

Having established the model of postnatal ZIKV infection of infant RMs and associated histopathology, our next objective was to investigate persistent brain structural consequences

of ZIKV infection using longitudinal MRI. Structural MRI brain scans were acquired from two ZIKV-infected infant RMs and two age-matched uninfected controls at three and six months of age. Due to the small sample size, MRI findings were considered descriptive in nature; however, a consistent effect was considered potentially clinically relevant. T1-weighted structural MRI revealed no differences between ZIKV-infected RMs and controls for total brain volume or intracranial volume, calculated as the sum of brain grey and white matter and CSF (Tables S2 and S3). However, the size of the lateral ventricles in the ZIKV-infected infant RMs was increased at both three and six months compared to controls (Fig. 5A,B and Fig. S4), despite the similar increases in total brain volume in both groups over time. When corrected for total brain volume, smaller white matter volume (Fig. 5B) paralleled by larger grey matter volume (Table S2) was found in ZIKV-infected RMs at both ages compared to controls.

The protracted postnatal development of brain areas important for socio-emotional behavior may make infants particularly vulnerable to ZIKV infection early in life. The hippocampus is one of the brain regions with extended postnatal development, doubling its volume from one week to two years of age in RMs (31, 32). Thus, the increase in total hippocampal volume between three and six months of age seen in the uninfected control infant RMs (Fig. 5B) is consistent with normative development in this species (18). However, ZIKV-infected infant RMs exhibited relatively blunted increases in hippocampal volume between three and six months of age (Fig. 5B). The amygdala volume, in contrast, did not differ in ZIKV-infected vs. control infant RMs at either age (Fig. 5B). Postnatal ZIKV infection resulted in a greater reduction in grey matter volume between three and six months in the right occipital lobe (Fig. 5B) and right temporal-visual cortex (Table S2) compared to age-matched uninfected controls. In summary, early postnatal ZIKV infection appears to be associated with specific brain maturational changes in cortical and subcortical regions evidenced by structural MRI.

Changes in brain functional connectivity: resting state functional MRI (rs-fMRI) analyses.

Rs-fMRI can be used to measure the FC between specific brain regions of interest (ROI) at rest, based on analysis of their temporal correlations of blood-oxygen-level dependent (BOLD) signal fluctuations. Utilizing this tool, we examined the impact of postnatal ZIKV infection on functional coupling/connectivity between ROIs during development, in addition to the brain structural impact reported in the previous section. The two ZIKV-infected infant RMs and two age-matched uninfected controls underwent rs-fMRI scans at three and six months of age. FC between ROIs were defined based on published anatomical parcellations (33, 34) mapped onto the UNC-Emory RM infant atlases registered to the F99 space (35). We first asked whether the blunted increase in hippocampal volume we detected in ZIKV-infected RMs would have a functional effect on hippocampal connectivity. Uninfected control infant RMs exhibited strengthening in positive FC between amygdala-hippocampus (right and left hemisphere) from three to six months of age (Fig. 6A,B). By contrast, ZIKV-infected infant RMs only exhibited this FC increase in the right hemisphere, whereas amygdala-hippocampus connectivity actually decreased in the left hemisphere from three to six months of age (Fig. 6B).

We next examined connections between the amygdala and hippocampus and the prefrontal cortex to better understand the impact of postnatal ZIKV infection on the limbic system network. Group differences in the directionality of FC were found between left amygdala-orbital frontal cortex (OFC) areas 11 and 13 (Fig. 6B), with ZIKV-infected infant RMs exhibiting positive connectivity at six months of age and uninfected controls demonstrating a negative connectivity at the same age. Weak connectivity was also observed between left hippocampus-OFC area 14 in ZIKV-infected RMs at both ages (with one of the infants showing uncoupling between these regions), whereas stronger negative connectivity developed in controls by six months (Fig. 6B). Lastly, ZIKV-infected infant RMs also showed changes in FC between visual cortical areas along the ventral motion pathway, that was of interest due to the potential for ZIKV to impact vision. FC between V3-middle temporal (MT) area in the right hemisphere increased from three to six months of age for ZIKV-infected RMs, but this trend was not detected in uninfected controls (Fig. 6B). All raw FC (r) values between ROIs are listed in Table S4. These results suggest that postnatal ZIKV infection caused not only histopathological alterations in the brain and quantifiable structural brain changes by MRI scan, but that some of the structural effects resulted in functional changes, in particular alterations in FC between limbic regions important for socio-emotional behavior.

Behavioral alterations after postnatal ZIKV infection: Human Intruder Paradigm.

We next sought to assess the impact of postnatal ZIKV infection on infant behavior and emotional reactivity. The Human Intruder (HI) Paradigm is a validated measure of the behavioral response to an acute stressor in nonhuman primates (Fig. 7A) (36-39) similar to the task used for assessing dispositional anxiety and behavioral inhibition in children (40). The HI task robustly quantifies emotional reactivity based on the salience of threat presented by the presence and gaze direction of the intruder (Table S5). Normally developing RM infants begin to modulate their emotional behavior responses based on the level of threat during the HI task at approximately four months of age (37, 39, 41), thus we first conducted testing at six months of age. Normally developing infant RMs exhibit increased freezing and avoid vocalizations when faced with the mild threat of the intruder's profile (Profile condition) as a defensive/anti-predator response. Subsequently, normally developing infant RMs exhibit increased hostility, anxiety, fear, and affiliative behaviors when faced with the more severe threat of the intruder's direct gaze (Stare condition). This species-typical behavioral response to the increasing level of threat was observed in the control infant RMs (Fig. 7B). However, the ZIKV-infected infant RMs did not freeze during any condition ($p=0.039$, $\eta_p^2=0.80$; Fig. 7B) and during Stare they expressed less hostility ($p=0.029$, $\eta_p^2=0.83$) and fewer anxiety behaviors ($p=0.001$, $\eta_p^2=0.97$) than controls (Fig. 7B). Additionally, ZIKV-infected RMs emitted more vocalizations and self-directed behaviors compared to controls during all conditions ($p=0.025$, $\eta_p^2=0.95$ and $p=0.011$, $\eta_p^2=0.98$, respectively; Fig. 7B).

These data, together with the neuronal changes in temporal lobe structures we observed by structural and rs-fMRI, suggest that postnatal ZIKV infection of infant RMs may disrupt the normal maturation of brain areas important for socio-emotional behavior, resulting in abnormal emotional processing. Correlations between rs-fMRI and emotional responses on

the HI paradigm were conducted to examine these potential relationships. Interestingly, a strong negative correlation was found for left amygdala-hippocampal FC and self-directed behaviors ($r=-0.98$, $p=0.006$; Fig. 7C), consistent with the previous finding that early hippocampal damage (and presumably decreased activity) results in increased self-directed behaviors on the HI paradigm (45). In addition, there was a strong negative correlation between left hippocampus-OFC area 14 FC and hostile behaviors ($r=-0.93$, $p=0.031$; Fig. 7C), indicating that the weak connectivity between these regions in ZIKV-infected RM infants may predict the decreased hostile behaviors on the HI task, since OFC 14 is involved in arousal and facial emotion recognition (42, 43).

Neonatal lesions to temporal lobe structures result in altered emotional behavior and changes in cortisol stress reactivity (38, 41). Since ZIKV-infected infant RMs exhibited structural and functional changes in temporal lobe structures, as well as altered emotional response, we examined stress reactivity using blood collected immediately before and after the acute stressor (HI task). Despite the structural and functional changes we observed in the brain in ZIKV-infected infants, they exhibited similar basal (pre-stress) cortisol concentrations and cortisol stress response (as measured by a percent change from pre- to post-stressor) as controls ($p=0.81$; Fig. 7B), suggesting that alterations following postnatal ZIKV infection occur in specific brain circuits regulating emotional responses, but not in the hypothalamic-pituitary-adrenal (HPA) axis at six months of age.

The HI Paradigm was repeated in the same animals at twelve months of age to examine whether the behavioral alterations we observed at six months were persistent. As shown in Fig. 7D, many of the atypical responses exhibited by the ZIKV-infected RMs continued, while the control RMs maintained a normal developmental response to this test of emotional reactivity. Specifically, at twelve months of age ZIKV-infected RMs continued to demonstrate less freezing during the profile condition ($p=0.018$, $\eta_p^2=0.96$; Fig. 7D) and to emit more vocalizations during all phases of the task compared to controls ($p=0.03$, $\eta_p^2=0.93$; Fig. 7D). Additionally, ZIKV-infected RMs continued to express less hostility during the Stare condition ($p=0.042$, $\eta_p^2=0.92$; Fig. 7D). Whereas at six months ZIKV-infected RMs had been less anxious and exhibited more self-directed behaviors compared to controls, at twelve months ZIKV-infected RMs did not differ from controls in terms of anxiety or self-directed behaviors, largely due to wide variations in behavior between the two animals (Fig. 7B, D). Both ZIKV-infected RMs demonstrated increased affiliative behaviors during the Stare condition compared to controls at twelve months ($p=0.035$, $\eta_p^2=0.81$; Fig. 7D), with a similar trend seen at six months of age (Fig. 7B). Examination of cortisol concentrations at twelve months of age revealed no difference between ZIKV-infected RMs and controls in the cortisol stress response, consistent with the findings at six months (Fig. 7B, D). Interestingly, mid-day basal (pre-stress) cortisol concentrations were lower in ZIKV-infected RMs compared to control RMs at twelve months of age ($p=0.022$; Fig. 7D), a finding that has been previously noted in macaques with neonatal hippocampal lesions and humans with hippocampal damage (41, 44).

Sparing of visual recognition memory after postnatal ZIKV infection: Visual Paired Comparison (VPC) task.

Since we observed structural, functional, and behavioral alterations related to the hippocampus following ZIKV infection, we next interrogated another function of the hippocampus, namely, memory. The visual paired comparison (VPC) task has been widely used to study the development of visual recognition memory in infant humans and macaques (45-48). Both ZIKV-infected infant RMs displayed the typical strong preference for novelty throughout the task (Fig. S5), indicating intact vision and recognition memory. Interestingly, one control animal displayed a delay-independent, equally strong preference either for the familiar or the novel across trials. Thus, to avoid bias, we analyzed the data as different from chance, rather than preference for novelty. Overall, performance between the two groups was similar with no effect of group ($p=0.34$), or of time ($p=0.106$), nor was the interaction of group x time significant ($p=0.08$).

Discussion

This study represents a longitudinal analysis of brain structure, function, and behavior following postnatal ZIKV infection of young infant primates during an important period of brain development. The majority of research in newborns and infants has to date focused on the congenital ZIKV syndrome (1-3, 49), leaving the outcome of early postnatal infection on the developing infant brain uncertain. Reports of microcephaly developing after birth with congenital ZIKV infection (50, 51) suggest that the postnatal insult of ZIKV to the developing brain can be severe.

We found that ZIKV displays replication kinetics in infant macaques that are similar to adult macaques and humans (28, 29, 52), and initially seeds the lymph nodes and spleen. By two weeks post infection, ZIKV had disseminated to the peripheral and central nervous systems of postnatally infected infants, as evidenced by the presence of viral nucleic acid and histopathologic changes. Consistent with prior work, our results suggest that ZIKV can infect cerebellar neurons and microglial cells (8, 53-61). Similar to the fetal brain injury observed after maternal ZIKV infection in a pigtail macaque model as well as congenital ZIKV syndrome in humans (2, 26, 62, 63), our analysis of postnatal ZIKV infection in RM infants revealed inflammation, reactive astrocytes, gliosis in the grey and white matter, axonal injury, and apoptosis in the brain and spinal cord. In particular, the consistent finding of astrogliosis between the infant infection model described here and fetal infection illustrates a common pathology of postnatal and *in utero* ZIKV infection (63). In our model, ZIKV RNA was not detected in the brain regions showing increased apoptosis and gliosis, suggesting these abnormalities may be due to an indirect inflammatory mechanism rather than direct cytopathic effect of the virus.

In adult macaques, ZIKV has been detected by PCR in multiple tissues, including brain, at day 35-72 post infection (64, 65). In addition, ZIKV was found in the CSF of an adult RM at 42 days after inoculation (64). Although we did not specifically attempt to measure virus at these later time points, the neuroimaging and behavioral abnormalities described in this work suggest that ZIKV may lead to long-term neurobehavioral damage to primate infants.

Whether these findings are due to immune events triggered during acute infection or to persistence of virus in the brain (or both) remains unknown.

Using structural MRI scans at three and six months of age, we observed a persistent reduction in white matter volume and increase in ventricular size in ZIKV-infected infant RMs as compared to age-matched controls. To our knowledge, normative MRI data regarding the volume of lateral ventricles in a larger sample of control RM infants matching our study conditions are not available. However, eleven female RM at three months of age and eighteen female RM at six months of age were imaged using similar protocols, as described in the UNC-Emory infant atlas (39), demonstrating a standard deviation of 56 mm³ for lateral ventricle volumes across this dam-reared social group. The difference in the volume of the lateral ventricles in ZIKV-infected RM compared to control RM in the present work was greater, with a mean at three months of 341 vs. 164 mm³ and at six months of 321 vs. 184 mm³. Thus, the difference we observed is not merely a variation from normal, but rather likely indicates a true enlargement of the ventricle size following postnatal ZIKV infection. Similar but more extensive ventriculomegaly typically of the lateral ventricles has been reported in live-born infants and autopsied fetuses following *in utero* ZIKV infection (1, 2, 66, 67), supporting a potentially similar underlying mechanism for these effects.

We also found blunted hippocampal volume growth in ZIKV-infected infant RMs as compared to controls. Specific damage to the hippocampus has also been noted in models of ZIKV-infected adult rodents (25) and can be explained by the protracted postnatal development of this brain region (18), making it vulnerable to postnatal insults. The structural impact to the hippocampus was paralleled by alterations in its FC with other limbic regions such as the amygdala and OFC, which also demonstrated an abnormal interaction on rs-fMRI, in ZIKV-infected infant RM. Importantly, the structural and functional brain changes we observed corresponded with changes in emotional behavior. While studies have demonstrated an impact of nursery-rearing on brain development and behavior (68, 69), rearing conditions and handling experiences were the same for control and ZIKV-infected RM infants in this study. ZIKV-infected infants were not impaired in their ability to produce emotional responses, but instead exhibited an atypical emotional response based on the salience of the threat presented. For example, ZIKV-infected infants consistently vocalized more and froze less than controls during the mild-threat of the intruder profile, yet exhibited less hostility during the salient-threat of the intruder stare. OFC area 14 has been implicated in arousal and facial emotion recognition (42, 43), and the weak connectivity between OFC 14 and the hippocampus seen in ZIKV-infected infant RMs may have resulted in less arousal and fewer hostile behaviors compared to uninfected controls. OFC 11 and 13 are involved in the ability to flexibly respond to rapidly changing social information, and cross-talk between the amygdala and OFC areas 11 and 13 guides optimal decision making (70). ZIKV-infected and control infant RM displayed opposite connectivity between these regions, possibly influencing the incorporation of new information into decisions, although this behavior was not specifically tested in this work. Neonatal lesions of the amygdala or hippocampus have resulted in similar behavioral changes exhibited by the ZIKV-infected infant RMs on the HI task in nursery-reared animals as well as in adolescents and adults in a social cohort (38, 41, 71-73). Damage to the hippocampus may also affect visual recognition memory (74). However, we found that

recognition memory at six months of age, as measured by the VPC task, was similar in ZIKV-infected RM infants and uninfected controls, indicating selective sparing of this function. Although performance on the VPC task in adults is impacted by hippocampal damage, a lack of memory deficit in infancy was also reported in animals with selective damage to the hippocampal formation (75) or exposure to anesthesia (45) that result in similar emotional changes (41, 76). Interestingly, RM infants with experimental selective hippocampal lesions evidenced a late-developing delay-dependent memory impairment as they reached adulthood (75), providing further rationale for longitudinal neurocognitive testing following postnatal ZIKV infection.

ZIKV has been linked with damage to the visual system, with ocular and brain visual system abnormalities seen in congenital ZIKV infection (50, 77, 78). Additionally, adults with Guillain-Barre Syndrome following ZIKV infection exhibit cytotoxic edema in the occipital lobe (79), the location of the visual cortex. We found that postnatal ZIKV infection in infant RM resulted in a greater reduction in grey matter volume between three and six months in the right occipital lobe and right temporal-visual cortex compared to age-matched uninfected controls, with abnormal inflammation, astrogliosis, and apoptosis apparent in the occipital cortex early in infection. Performance on the VPC task, however, confirmed intact visual processes necessary to encode and recognize a visual stimulus in ZIKV-infected RM infants.

There were limitations to this study. First, a small number of animals was studied; therefore, comparisons between groups are descriptive in nature. The strength of these results does not reside in statistical significance, but rather in the effect size and potential clinical relevance of this work. In fact, the National Institutes of Health recently funded a study of neurodevelopmental outcomes of Guatemalan infants and children infected with ZIKV after birth (80), that may replicate our findings and/or provide new insights into postnatal ZIKV infection. Second, our results reflect infection with a single dose of a single ZIKV isolate. The PRVABC59 strain of ZIKV is an Asian genotype virus that has been widely used for RM studies and is most closely related to isolates from Brazil (81), where the largest outbreak of ZIKV infection has occurred to date. Additional work to substantiate our findings regarding postnatal ZIKV infection should utilize a larger cohort of infant RMs infected with multiple virus isolates that reflect the diversity of current infections. Third, it should be noted that rs-fMRI has several limitations: (i) FC was obtained under anesthesia, but we note that isoflurane doses were kept below those employed in previous studies reporting patterns of coherent BOLD fluctuations similar to the awake state, including in sensory and visual systems (82-85); (ii) only female subjects were studied and there may be sex differences in the impact of ZIKV infection on FC brain development; and (iii) it is difficult to relate changes in strength or direction of FC between cortical areas with specific physiological, cellular, or molecular brain maturational processes, which will need to be addressed in future studies with larger sample sizes.

In summary, early postnatal ZIKV infection appears to be associated with histopathologic, behavioral, and brain structural and functional abnormalities during the first year of life. The impact of early postnatal ZIKV infection during later stages of life (e.g., school age, adolescence) remains unknown. Previous research using macaques with hippocampal lesions made in the neonatal period demonstrated schizophrenic-like characteristics that only

manifested during adolescence (86). Further, studies of postnatally acquired CMV revealed that some of the cognitive sequelae do not become evident until school age (22). Our finding that postnatal ZIKV infection of infant RMs causes persistent changes consistent with delayed or dysfunctional brain maturation suggest that long-term clinical monitoring of all ZIKV-infected infants and children may be critical. Heightened surveillance of this population, with attention to neurodevelopment and behavior, is warranted. This RM model sheds insight into potential outcomes of human infants infected with ZIKV postnatally and provides a platform with which to test therapeutic approaches to alleviate the neurologic consequences of ZIKV infection.

Materials and Methods

Study Design

Animals.—This study was conducted in strict accordance with USDA regulations and the recommendations in the Guide for the Care and Use of Laboratory Animals of the National Institutes of Health, was approved by the Emory University Institutional Animal Care and Use Committee (AWA# A3180-01), and conducted in an AAALAC accredited facility. Eight infant Indian RM (*Macaca mulatta*) including two males and six females were used in this study. The infants were delivered naturally by their dams while housed in indoor/outdoor social groups. Infants were then removed from their dams at 5-10 days of age and transported to the Yerkes National Primate Research Center (YNPRC) nursery facility. All infants were singly housed in warming incubators for the first 3-4 weeks. Infants were hand fed formula every 2-3 hours for the first month, then via self-feeders for the next three months as per standard YNPRC protocol. Soft blankets, plush toys or fleece were provided and changed daily. Soft chow and fruits were introduced starting at one month of age, and by four months, formula was discontinued and all were fed a diet of Purina Primate Chow, Old World Monkey formulation, supplemented with daily fruits and vegetables. Water was provided ad libitum. At four weeks of age, infants transitioned into age-appropriate caging with visual and auditory contact with conspecifics. At 6-7 weeks of age they began socialization consisting of protected contact housing supplemented with 2-3 hours daily of full contact with their age-matched peer. By three months of age, each pair was housed entirely together. ZIKV-infected infants were housed in an ABSL-2+ room until cleared of virus in blood and urine. Control infants were initially housed in a separate ABSL-2 room and then all infant pairs were housed together after ZIKV clearance with visual contact to increase visual socialization and control for environmental factors.

Virus and infection.—The ZIKV of Puerto Rican origin (PRVABC59, GeneBank accession number: KU501215.1) used in this study had been passaged four times and titered on Vero cells. Experimental infections were performed via the subcutaneous (sc) route using 10^5 plaque forming units (pfu) of ZIKV PRVABC59.

ZIKV RNA detection by qRT-PCR.—Total RNA was extracted from 140ul plasma and CSF samples using the QIAamp Viral RNA Mini Kit (Qiagen). RNA from urine and saliva was isolated using the QIAamp Circulating Nucleic Acid Kit (Qiagen) for the extraction of larger volumes (up to 3 ml). Tissues were suspended in TRI reagent and mechanically

homogenized using beads. Total RNA was isolated from homogenized tissues using the Direct-zol RNA MiniPrep Plus Kit (Zymo Research) per the manufacturer's instructions. ZIKV RNA standard was generated by annealing two oligonucleotides spanning the target ZIKV prM-E gene region and performing *in vitro* transcription using the MEGAscript T3 Transcription Kit (Ambion). Purified RNA was reverse transcribed using the High-Capacity cDNA Reverse Transcription Kit (Applied Biosystems) and random hexamers. For quantitation of viral RNA, a standard curve was generated using tenfold dilutions of ZIKV RNA standard, and qRT-PCR was performed using TaqMan Gene Expression Master Mix (Applied Biosystems) and ZIKV primers (1 μ M) and probe (250 nM). The ZIKV primer-probe set targeting the prM-E gene region included forward primer ZIKV/PR 907 (5'-TTG GTC ATG ATA CTG CTG ATT GC-3'), reverse primer ZIKV/PR 983c (5'- CCT TCC ACA AAG TCC CTA TTG C-3'), and probe ZIKV/PR 932 FAM (5'- CGG CAT ACA GCA TCA GGT GCA TAG GAG-3'). The probe was labeled with 6-carboxyfluorescein (FAM) at the 5' end and two quenchers, an internal ZEN quencher and 3' end Iowa Black FQ (IDT). The standard curve had a R^2 value greater than 0.99. Viral RNA copies were interpolated from the standard curve using the sample C_T value. For tissue samples, viral RNA copies were normalized to RNA input (μ g RNA). For plasma samples, viral RNA copies were represented as copies per ml plasma.

ZIKV RNA *in situ* hybridization (ISH).—ZIKV ISH was done on cerebellum and cauda equina using riboprobes that target multiple genes of ZIKV strains including PRVABC59 (Advanced Cell Diagnostics). RNAscope was performed as per manufacturer's recommended protocol. Briefly, prepared slides were baked for 1 h at 60°C prior to use. After deparaffinization and hydration, tissue slides were air-dried and treated with a peroxidase blocker before heating in a target retrieval solution for 20 min at 95–100°C. Protease was then applied for 30 min at 40°C. Target probes were hybridized for 2 h at 40°C, followed by a series of signal amplification and washing steps. Red chromogen development was performed following the RNAscope 2.5 HD detection protocol and reagents. The chromogenic detection was performed using FastRed as substrate to generate red signal followed by counterstaining with hematoxylin.

Immunohistochemistry.—ZIKV-infected RM sacrificed on day 3 and day 14–15 p.i. were subjected to histopathologic analyses. For histopathologic examination, various tissue samples were fixed in 10% neutral buffered formalin, paraffin-embedded, sectioned at 5 μ m, and stained with hematoxylin and eosin (H&E). To define specific cell types, we performed immunohistochemistry (IHC) analysis by using antibodies against glial fibrillary acidic protein (GFAP, Agilent Technologies, M0761), and Caspase-3 (Cell Signaling, 9662). IHC staining on sections of brain from both ZIKV-infected and uninfected animals was performed using a biotin-free polymer system (Biocare Medical). The paraffin-embedded sections were subjected to deparaffinization in xylene, rehydration in graded series of ethanol, and rinsed with double distilled water. The brain sections were incubated with rabbit anti-human GFAP and Caspase-3 antibodies for 1h after heat-induced epitope retrieval. Antibody labelling was visualized by development of the chromogen (Warp Red or DAB Chromogen Kits; Biocare Medical). Digital images of brain were captured at 100x and

200x magnification with an Olympus BX43 microscope equipped with a digital camera (DP26, Olympus) and evaluated using Cellsens digital imaging software 1.15 (Olympus).

MRI studies.—Neuroimaging data were collected longitudinally at three and six months of age using a Siemens 3T Tim Trio system (Siemens Medical Solutions) with a Tx/Rx 8-channel volume coil. Data were acquired in a single session, which included T1- and T2-weighted structural scans, and two 15 minute rs-fMRI (T2*-weighted) scans to measure temporal changes in regional blood-oxygen-level dependent (BOLD) signal. Animals were scanned in the supine position in the same orientation, achieved by placement and immobilization of the head in a custom-made head holder via ear bars and a mouthpiece. Following initial telazol induction and intubation, scans were collected under isoflurane anesthesia (0.8-1% to effect), kept at the lowest dose possible to minimize effects of anesthesia on BOLD signal (82-85). End-tidal CO₂, inhaled CO₂, O₂ saturation, heart rate, respiratory rate, blood pressure, and body temperature were monitored continuously and maintained during each MRI session.

Structural MRI acquisition: High-resolution T1-weighted scans were acquired for volumetrics and registration of the functional scans using a 3D magnetization prepared rapid gradient echo (3D-MPRAGE) parallel image sequence (TR/TE = 2600/3.46msec, FOV: 116mm × 116mm, voxel size: 0.5mm³ isotropic, 8 averages) with GRAPPA acceleration factor of R = 2). T2-weighted MRI scans were collected using a 3D fast spin-echo sequence (TR/TE = 3200/373msec, FOV: 128mm × 128mm, voxel size: 0.5mm³ isotropic, 3 averages) with GRAPPA (R=2) to aid with registration and delineation of anatomical borders.

Structural MRI data processing and analysis: Datasets were processed using AutoSeg_3.3.2 segmentation package (87) to get the volumes of brain white matter (WM), gray matter (GM), cerebrospinal fluid (CSF), cortical (temporal visual area, temporal auditory area, prefrontal, frontal, parietal and occipital lobes) and subcortical (hippocampus, amygdala) brain areas. Image processing steps included: 1) averaging T1 and T2 images to improve signal-to-noise ratio, 2) intensity inhomogeneity correction, 3) rigid body registration of the subject MRI to the three or the six months UNC-Emory infant RM atlases (35), 4) tissue segmentation and skull-stripping, 5) registration of the atlas to the subject's brain to generate cortical parcellations (affine followed by deformable SyN/ANTS registration), 6) manual editing of the amygdala and hippocampus was done on all scans using previously published neuroanatomical boundaries (31). For more detailed description of the structural MRI analysis, see (87, 88). Cortical and subcortical volume measurements (mm³) were corrected by total brain volume (TBV) then multiplied by 100 (e.g., hippocampal volume/TBV × 100).

Rs-fMRI acquisition: BOLD-weighted functional images were collected using a single-shot echo-planar imaging (EPI) sequence (400 volumes, TR/TE = 2060/25msec, 2×15min, voxel size: 1.5mm³ isotropic) following the T1-MRI scan. An additional short, reverse-phase encoding scan was also acquired for unwarping susceptibility-induced distortions in the EPI images using previously validated methods (89).

Functional MRI data pre-processing: Imaging data was pre-processed with an in-house pipeline in Nipype (90) with modifications (91-94), including adaptations for the RM brain (95). After the EPI functional time series were concatenated and rigid-body registered to the subject's T1-weighted structural image, this was transformed to conform to age-specific T1-weighted RM infant atlases (35) using non-linear registration methods in FSL (FNIRT). These atlases were registered to the 112RM-SL atlas in F99 space (96, 97). We registered the scans to the age-specific appropriate infant atlas (three or six months). Frames with displacement (FD) values greater than 0.2 mm were removed (98, 99) and data were visually inspected upon preprocessing completion to exclude series with unsatisfactory co-registration or significant BOLD signal dropout.

Functional Connectivity Analysis: FC between regions of interest (ROIs) including the amygdala, hippocampus, orbital frontal cortex (OFC), and visual areas (V1, V3, Middle Temporal area [MT]) were analyzed. ROIs were defined based on published anatomical parcellations (33, 34) mapped onto the UNC-Emory RM infant atlases registered to the F99 space (35). The left and right amygdala label maps were manually drawn by experts using cytoarchitectonic maps in the existing UNC-Wisconsin adolescent atlas (100) and other ROIs were manually edited in the infant atlases following established anatomical landmarks (101, 102). The time course of the BOLD signal was averaged across all voxels within each ROI using a single ROI as the seed, and then correlated with the time course of the other ROIs. FC values are calculated as correlation coefficients (r-values) between ROIs BOLD time courses, were extracted from correlation matrices using Matlab (MathWorks, Inc.).

HI Paradigm.—Infants were previously trained to quickly transfer from their home cage to a transport box. On the testing day, the subject was separated from the cagemate and transported from the nursery to a novel testing room where a basal blood sample (1 ml, awake femoral venipuncture) was collected within 10 min of initial disturbance, reflecting baseline concentrations of plasma biomarkers. The RM was then placed in a modified housing wire-mesh cage with one side in clear acrylic to allow video recording of animal's behavior. The paradigm consisted of three conditions: Alone condition: animal remained alone in the cage for 9 minutes to acclimate to the environment and obtain a baseline measure of behavior. Profile condition: a human intruder (researcher wearing a rubber mask) entered the room, sat on a stool two meters from the test cage, while presenting his profile (without eye contact) to the animal for 9 minutes. Then the intruder left the room giving the animal a 3 min break. Stare condition: the human intruder re-entered the room but this time stared directly at the animal for 9 minutes. A second blood draw was collected (1 ml, awake femoral draw) immediately following the task, reflecting concentrations of plasma biomarkers in response to acute stress. Blood samples were collected in pre-chilled plastic 2 ml vacutainer tubes containing EDTA and immediately placed on ice. Samples were centrifuged at 3000rpm for 15min in a refrigerated centrifuge (at 4°C). Plasma was pipetted into sterile tubes and stored at -80°C until assayed.

Statistical Analysis

HI paradigm analyses were conducted using SPSS 24 for Windows (IBM Corporation) and significance was set at $p < 0.05$. Group differences in emotional behaviors were examined

with repeated measures ANOVA with Group (control, ZIKV) as the between subjects factor and Condition (Alone, Profile, Stare) as the within subject repeated measures. Effect sizes were calculated using partial eta squared (η_p^2). Emotional reactivity to the intruder was assessed via videotape recording for later coding using the Observer XT 10 software (Noldus, Inc.) and a detailed ethogram (Table S4). Two blinded experimenters coded all of the videotapes but had a high degree of interrater reliability Cohen's $\kappa = 0.86$ and an average intrarater reliability of Cohen's $\kappa = 0.97$. Pearson correlation coefficient was used to assess for association between behavior on HI task and FC. Cortisol assay was analyzed by Independent T-tests with Group (control, ZIKV) as the between subject factor and percent change in cortisol concentration as the dependent variable.

Supplementary Material

Refer to Web version on PubMed Central for supplementary material.

Acknowledgements

We thank S. Ehnert and the YNPRC Division of Research Resources for expert assistance with animal procedures, M. Thompson and the Emory Environmental Health and Safety Office for supervising environmental infection control in the YNPRC nursery, and A. McElroy for training and helpful discussions. We would like to acknowledge Kristina De Paris from the University of North Carolina and Koen Van Rompay from the California National Primate Research Center (CNPRC) for providing control infant brains for histopathology (Grant numbers R01 DE022287 and R01 DE019064 to K.D.P. and P51 OD011107 to CNPRC).

Funding: This work was supported by the Pilot Grant Program of the YNPRC (P51 OD011132), the Emory Center for Childhood Infections and Vaccines, and Children's Healthcare of Atlanta. Research reported in this publication was supported by the National Library of Medicine of the National Institutes of Health under Award Number T15LM007088 (to E. F.). The content is solely the responsibility of the authors and does not necessarily represent the official views of the National Institutes of Health.

References and Notes

1. Brasil P, Pereira JP, Jr., Moreira ME, Ribeiro Nogueira RM, Damasceno L, Wakimoto M, Rabello RS, Valderramos SG, Halai UA, Salles TS, Zin AA, Horovitz D, Daltro P, Boechat M, Raja Gabaglia C, Carvalho de Sequeira P, Pilotto JH, Medialdea-Carrera R, Cotrim da Cunha D, Abreu de Carvalho LM, Pone M, Machado Siqueira A, Calvet GA, Rodrigues Baiao AE, Neves ES, Nassar de Carvalho PR, Hasue RH, Marschik PB, Einspieler C, Janzen C, Cherry JD, Bispo de Filippis AM, Nielsen-Saines K, Zika Virus Infection in Pregnant Women in Rio de Janeiro. *N Engl J Med* 375, 2321–2334 (2016). [PubMed: 26943629]
2. Mlakar J, Korva M, Tul N, Popovic M, Poljsak-Prijatelj M, Mraz J, Kolenc M, Resman Rus K, Vesnaver Vipotnik T, Fabjan Vodusek V, Vizjak A, Pizem J, Petrovec M, Avsic Zupanc T, Zika Virus Associated with Microcephaly. *N Engl J Med* 374, 951–958 (2016). [PubMed: 26862926]
3. Moore CA, Staples JE, Dobyns WB, Pessoa A, Ventura CV, Fonseca EB, Ribeiro EM, Ventura LO, Neto NN, Arena JF, Rasmussen SA, Characterizing the Pattern of Anomalies in Congenital Zika Syndrome for Pediatric Clinicians. *JAMA Pediatr*, (2016).
4. Dick GW, Kitchen SF, Haddow AJ, Zika virus. I. Isolations and serological specificity. *Trans R Soc Trop Med Hyg* 46, 509–520 (1952). [PubMed: 12995440]
5. Smithburn KC, Neutralizing antibodies against certain recently isolated viruses in the sera of human beings residing in East Africa. *J Immunol* 69, 223–234 (1952). [PubMed: 14946416]
6. Weinbren MP, Williams MC, Zika virus: further isolations in the Zika area, and some studies on the strains isolated. *Trans R Soc Trop Med Hyg* 52, 263–268 (1958). [PubMed: 13556872]
7. Haddow AJ, Williams MC, Woodall JP, Simpson DI, Goma LK, Twelve Isolations of Zika Virus from *Aedes (Stegomyia) Africanus (Theobald)* Taken in and above a Uganda Forest. *Bull World Health Organ* 31, 57–69 (1964). [PubMed: 14230895]

8. Dick GW, Zika virus. II. Pathogenicity and physical properties. *Trans R Soc Trop Med Hyg* 46, 521–534 (1952). [PubMed: 12995441]
9. Gulland A, Zika virus is a global public health emergency, declares WHO. *BMJ* 352, i657 (2016). [PubMed: 26839247]
10. Cugola FR, Fernandes IR, Russo FB, Freitas BC, Dias JL, Guimaraes KP, Benazzato C, Almeida N, Pignatari GC, Romero S, Polonio CM, Cunha I, Freitas CL, Brandao WN, Rossato C, Andrade DG, Faria Dde P, Garcez AT, Buchpiguel CA, Braconi CT, Mendes E, Sall AA, Zanotto PM, Peron JP, Muotri AR, Beltrao-Braga PC, The Brazilian Zika virus strain causes birth defects in experimental models. *Nature* 534, 267–271 (2016). [PubMed: 27279226]
11. Franca GV, Schuler-Faccini L, Oliveira WK, Henriques CM, Carmo EH, Pedi VD, Nunes ML, Castro MC, Serruya S, Silveira MF, Barros FC, Victora CG, Congenital Zika virus syndrome in Brazil: a case series of the first 1501 livebirths with complete investigation. *Lancet* 388, 891–897 (2016). [PubMed: 27372398]
12. Malkki H, CNS infections: Mouse studies confirm the link between Zika virus infection and microcephaly. *Nat Rev Neurol* 12, 369 (2016). [PubMed: 27231186]
13. Rasmussen SA, Jamieson DJ, Honein MA, Petersen LR, Zika Virus and Birth Defects--Reviewing the Evidence for Causality. *N Engl J Med* 374, 1981–1987 (2016). [PubMed: 27074377]
14. Glantz LA, Gilmore JH, Hamer RM, Lieberman JA, Jarskog LF, Synaptophysin and postsynaptic density protein 95 in the human prefrontal cortex from mid-gestation into early adulthood. *Neuroscience* 149, 582–591 (2007). [PubMed: 17916412]
15. Huttenlocher PR, Dabholkar AS, Regional differences in synaptogenesis in human cerebral cortex. *J Comp Neurol* 387, 167–178 (1997). [PubMed: 9336221]
16. Knickmeyer RC, Gouttard S, Kang C, Evans D, Wilber K, Smith JK, Hamer RM, Lin W, Gerig G, Gilmore JH, A structural MRI study of human brain development from birth to 2 years. *J Neurosci* 28, 12176–12182 (2008). [PubMed: 19020011]
17. Miller DJ, Duka T, Stimpson CD, Schapiro SJ, Baze WB, McArthur MJ, Fobbs AJ, Sousa AM, Sestan N, Wildman DE, Lipovich L, Kuzawa CW, Hof PR, Sherwood CC, Prolonged myelination in human neocortical evolution. *Proc Natl Acad Sci U S A* 109, 16480–16485 (2012). [PubMed: 23012402]
18. Lavenex P, Banta Lavenex P, Amaral DG, Postnatal development of the primate hippocampal formation. *Dev Neurosci* 29, 179–192 (2007). [PubMed: 17148960]
19. Bianchi S, Stimpson CD, Duka T, Larsen MD, Janssen WG, Collins Z, Bauernfeind AL, Schapiro SJ, Baze WB, McArthur MJ, Hopkins WD, Wildman DE, Lipovich L, Kuzawa CW, Jacobs B, Hof PR, Sherwood CC, Synaptogenesis and development of pyramidal neuron dendritic morphology in the chimpanzee neocortex resembles humans. *Proc Natl Acad Sci U S A* 110 Suppl 2, 10395–10401 (2013). [PubMed: 23754422]
20. Cooper ER, Hanson C, Diaz C, Mendez H, Abboud R, Nugent R, Pitt J, Rich K, Rodriguez EM, Smeriglio V, Encephalopathy and progression of human immunodeficiency virus disease in a cohort of children with perinatally acquired human immunodeficiency virus infection. *Women and Infants Transmission Study Group. J Pediatr* 132, 808–812 (1998). [PubMed: 9602190]
21. Epstein LG, Sharer LR, Goudsmit J, Neurological and neuropathological features of human immunodeficiency virus infection in children. *Ann Neurol* 23 Suppl, S19–23 (1988). [PubMed: 3279902]
22. Hamprecht K, Goelz R, Postnatal Cytomegalovirus Infection Through Human Milk in Preterm Infants: Transmission, Clinical Presentation, and Prevention. *Clin Perinatol* 44, 121–130 (2017). [PubMed: 28159200]
23. Goodman AB, Dziuban EJ, Powell K, Bitsko RH, Langley G, Lindsey N, Franks JL, Russell K, Dasgupta S, Barfield WD, Odom E, Kahn E, Martin S, Fischer M, Staples JE, Characteristics of Children Aged <18 Years with Zika Virus Disease Acquired Postnatally - U.S. States, January 2015–July 2016. *MMWR Morb Mortal Wkly Rep* 65, 1082–1085 (2016). [PubMed: 27711041]
24. Li J, Chong CY, Tan NW, Yung CF, Tee NW, Cheng Thoon K, Characteristics of Zika virus disease in children: Clinical, hematological and virological findings from an outbreak in Singapore. *Clin Infect Dis*, (2017).

25. Li H, Saucedo-Cuevas L, Regla-Nava JA, Chai G, Sheets N, Tang W, Terskikh AV, Shresta S, Gleeson JG, Zika Virus Infects Neural Progenitors in the Adult Mouse Brain and Alters Proliferation. *Cell Stem Cell* 19, 593–598 (2016). [PubMed: 27545505]
26. Adams Waldorf KM, Stencel-Baerenwald JE, Kapur RP, Studholme C, Boldenow E, Vornhagen J, Baldessari A, Dighe MK, Thiel J, Merrillat S, Armistead B, Tisoncik-Go J, Green RR, Davis MA, Dewey EC, Fairgrieve MR, Gatenby JC, Richards T, Garden GA, Diamond MS, Juul SE, Grant RF, Kuller L, Shaw DW, Ogle J, Gough GM, Lee W, English C, Hevner RF, Dobyns WB, Gale M, Jr., Rajagopal L, Fetal brain lesions after subcutaneous inoculation of Zika virus in a pregnant nonhuman primate. *Nat Med* 22, 1256–1259 (2016). [PubMed: 27618651]
27. Coffey LL, Pesavento PA, Keesler RI, Singapuri A, Watanabe J, Watanabe R, Yee J, Bliss-Moreau E, Cruzen C, Christe KL, Reader JR, von Morgenland W, Gibbons AM, Allen AM, Linnen J, Gao K, Delwart E, Simmons G, Stone M, Lanteri M, Bakkour S, Busch M, Morrison J, Van Rompay KK, Zika Virus Tissue and Blood Compartmentalization in Acute Infection of Rhesus Macaques. *PLoS One* 12, e0171148 (2017). [PubMed: 28141843]
28. Dudley DM, Aliota MT, Mohr EL, Weiler AM, Lehrer-Brey G, Weisgrau KL, Mohns MS, Breitbach ME, Rasheed MN, Newman CM, Gellerup DD, Moncla LH, Post J, Schultz-Darken N, Schotzko ML, Hayes JM, Eudailey JA, Moody MA, Permar SR, O'Connor SL, Rakasz EG, Simmons HA, Capuano S, Golos TG, Osorio JE, Friedrich TC, O'Connor DH, A rhesus macaque model of Asian-lineage Zika virus infection. *Nat Commun* 7, 12204 (2016). [PubMed: 27352279]
29. Osuna CE, Lim SY, Deleage C, Griffin BD, Stein D, Schroeder LT, Omange R, Best K, Luo M, Hraber PT, Andersen-Elyard H, Ojeda EF, Huang S, Vanlandingham DL, Higgs S, Perelson AS, Estes JD, Safronetz D, Lewis MG, Whitney JB, Zika viral dynamics and shedding in rhesus and cynomolgus macaques. *Nat Med* 22, 1448–1455 (2016). [PubMed: 27694931]
30. Priyamvada L, Cho A, Onlamoon N, Zheng NY, Huang M, Kovalenkov Y, Chokephaibulkit K, Angkasekwinai N, Pattanapanyasat K, Ahmed R, Wilson PC, Wrammert J, B Cell Responses during Secondary Dengue Virus Infection Are Dominated by Highly Cross-Reactive, Memory-Derived Plasmablasts. *J Virol* 90, 5574–5585 (2016). [PubMed: 27030262]
31. Payne C, Machado CJ, Bliwise NG, Bachevalier J, Maturation of the hippocampal formation and amygdala in *Macaca mulatta*: a volumetric magnetic resonance imaging study. *Hippocampus* 20, 922–935 (2010). [PubMed: 19739247]
32. Hunsaker MR, Scott JA, Bauman MD, Schumann CM, Amaral DG, Postnatal development of the hippocampus in the Rhesus macaque (*Macaca mulatta*): a longitudinal magnetic resonance imaging study. *Hippocampus* 24, 794–807 (2014). [PubMed: 24648155]
33. Lewis JW, Van Essen DC, Corticocortical connections of visual, sensorimotor, and multimodal processing areas in the parietal lobe of the macaque monkey. *J Comp Neurol* 428, 112–137 (2000). [PubMed: 11058227]
34. Markov NT, Ercsey-Ravasz MM, Ribeiro Gomes AR, Lamy C, Magrou L, Vezoli J, Misery P, Falchier A, Quilodran R, Gariel MA, Sallet J, Gamanut R, Huissoud C, Clavagnier S, Giroud P, Sappey-Marinié D, Barone P, Dehay C, Toroczka Z, Knoblauch K, Van Essen DC, Kennedy H, A weighted and directed interareal connectivity matrix for macaque cerebral cortex. *Cereb Cortex* 24, 17–36 (2014). [PubMed: 23010748]
35. Shi Y, Budin F, Yapuncich E, Rumble A, Young JT, Payne C, Zhang X, Hu X, Godfrey J, Howell B, Sanchez MM, Styner MA, UNC-Emory Infant Atlases for Macaque Brain Image Analysis: Postnatal Brain Development through 12 Months. *Front Neurosci* 10, 617 (2016). [PubMed: 28119564]
36. Coleman K, Pierre PJ, Assessing anxiety in nonhuman primates. *ILAR J* 55, 333–346 (2014). [PubMed: 25225310]
37. Kalin NH, Shelton SE, Defensive behaviors in infant rhesus monkeys: environmental cues and neurochemical regulation. *Science* 243, 1718–1721 (1989). [PubMed: 2564702]
38. Raper J, Wallen K, Sanchez MM, Stephens SB, Henry A, Villareal T, Bachevalier J, Sex-dependent role of the amygdala in the development of emotional and neuroendocrine reactivity to threatening stimuli in infant and juvenile rhesus monkeys. *Horm Behav* 63, 646–658 (2013). [PubMed: 23380162]

39. Raper J, Wilson M, Sanchez M, Machado CJ, Bachevalier J, Pervasive alterations of emotional and neuroendocrine responses to an acute stressor after neonatal amygdala lesions in rhesus monkeys. *Psychoneuroendocrinology* 38, 1021–1035 (2013). [PubMed: 23148887]
40. Kagan J, Reznick JS, Snidman N, Biological bases of childhood shyness. *Science* 240, 167–171 (1988). [PubMed: 3353713]
41. Raper J, Wilson M, Sanchez M, Payne C, Bachevalier J, Increased anxiety-like behaviors, but blunted cortisol stress response after neonatal hippocampal lesions in monkeys. *Psychoneuroendocrinology* 76, 57–66 (2017). [PubMed: 27888771]
42. Bechara A, Disturbances of emotion regulation after focal brain lesions. *Int Rev Neurobiol* 62, 159–193 (2004). [PubMed: 15530572]
43. Heberlein AS, Padon AA, Gillihan SJ, Farah MJ, Fellows LK, Ventromedial frontal lobe plays a critical role in facial emotion recognition. *J Cogn Neurosci* 20, 721–733 (2008). [PubMed: 18052791]
44. Buchanan TW, Kern S, Allen JS, Tranel D, Kirschbaum C, Circadian regulation of cortisol after hippocampal damage in humans. *Biol Psychiatry* 56, 651–656 (2004). [PubMed: 15522248]
45. Alvarado MC, Murphy KL, Baxter MG, Visual recognition memory is impaired in rhesus monkeys repeatedly exposed to sevoflurane in infancy. *Br J Anaesth* 119, 517–523 (2017). [PubMed: 28575197]
46. Burbacher TM, Grant KS, Measuring infant memory: Utility of the visual paired-comparison test paradigm for studies in developmental neurotoxicology. *Neurotoxicol Teratol* 34, 473–480 (2012). [PubMed: 22750243]
47. Fagan JF, 3rd, Memory in the infant. *J Exp Child Psychol* 9, 217–226 (1970). [PubMed: 5452116]
48. Fantz RL, Visual Experience in Infants: Decreased Attention to Familiar Patterns Relative to Novel Ones. *Science* 146, 668–670 (1964). [PubMed: 14191712]
49. Russo FB, Jungmann P, Beltrao-Braga PCB, Zika infection and the development of neurological defects. *Cell Microbiol* 19, (2017).
50. Aragao M, Holanda AC, Brainer-Lima AM, Petribu NCL, Castillo M, van der Linden V, Serpa SC, Tenorio AG, Travassos PTC, Cordeiro MT, Sarteschi C, Valenca MM, Costello A, Nonmicrocephalic Infants with Congenital Zika Syndrome Suspected Only after Neuroimaging Evaluation Compared with Those with Microcephaly at Birth and Postnatally: How Large Is the Zika Virus "Iceberg"? *AJNR Am J Neuroradiol* 38, 1427–1434 (2017). [PubMed: 28522665]
51. van der Linden V, Pessoa A, Dobyns W, Barkovich AJ, Junior HV, Filho EL, Ribeiro EM, Leal MC, Coimbra PP, Aragao MF, Vercosa I, Ventura C, Ramos RC, Cruz DD, Cordeiro MT, Mota VM, Dott M, Hillard C, Moore CA, Description of 13 Infants Born During October 2015-January 2016 With Congenital Zika Virus Infection Without Microcephaly at Birth - Brazil. *MMWR Morb Mortal Wkly Rep* 65, 1343–1348 (2016). [PubMed: 27906905]
52. Paz-Bailey G, Rosenberg ES, Doyle K, Munoz-Jordan J, Santiago GA, Klein L, Perez-Padilla J, Medina FA, Waterman SH, Gubern CG, Alvarado LI, Sharp TM, Persistence of Zika Virus in Body Fluids - Preliminary Report. *N Engl J Med*, (2017).
53. Bell TM, Field EJ, Narang HK, Zika virus infection of the central nervous system of mice. *Arch Gesamte Virusforsch* 35, 183–193 (1971). [PubMed: 5002906]
54. Gabriel E, Ramani A, Karow U, Gottardo M, Natarajan K, Gooi LM, Goranci-Buzhala G, Krut O, Peters F, Nikolic M, Kuivanen S, Korhonen E, Smura T, Vapalahti O, Papantonis A, Schmidt-Chanasit J, Riparbelli M, Callaini G, Kronke M, Utermohlen O, Gopalakrishnan J, Recent Zika Virus Isolates Induce Premature Differentiation of Neural Progenitors in Human Brain Organoids. *Cell Stem Cell* 20, 397–406 e395 (2017). [PubMed: 28132835]
55. Li C, Xu D, Ye Q, Hong S, Jiang Y, Liu X, Zhang N, Shi L, Qin CF, Xu Z, Zika Virus Disrupts Neural Progenitor Development and Leads to Microcephaly in Mice. *Cell Stem Cell* 19, 120–126 (2016). [PubMed: 27179424]
56. Noronha L, Zanluca C, Azevedo ML, Luz KG, Santos CN, Zika virus damages the human placental barrier and presents marked fetal neurotropism. *Mem Inst Oswaldo Cruz* 111, 287–293 (2016). [PubMed: 27143490]
57. Qian X, Nguyen HN, Song MM, Hadiono C, Ogden SC, Hammack C, Yao B, Hamersky GR, Jacob F, Zhong C, Yoon KJ, Jeang W, Lin L, Li Y, Thakor J, Berg DA, Zhang C, Kang E,

- Chickering M, Nauen D, Ho CY, Wen Z, Christian KM, Shi PY, Maher BJ, Wu H, Jin P, Tang H, Song H, Ming GL, Brain-Region-Specific Organoids Using Mini-bioreactors for Modeling ZIKV Exposure. *Cell* 165, 1238–1254 (2016). [PubMed: 27118425]
58. Retallack H, Di Lullo E, Arias C, Knopp KA, Laurie MT, Sandoval-Espinosa C, Mancina Leon WR, Krencik R, Ullian EM, Spatazza J, Pollen AA, Mandel-Brehm C, Nowakowski TJ, Kriegstein AR, DeRisi JL, Zika virus cell tropism in the developing human brain and inhibition by azithromycin. *Proc Natl Acad Sci U S A* 113, 14408–14413 (2016). [PubMed: 27911847]
59. Souza BS, Sampaio GL, Pereira CS, Campos GS, Sardi SI, Freitas LA, Figueira CP, Paredes BD, Nonaka CK, Azevedo CM, Rocha VP, Bandeira AC, Mendez-Otero R, Dos Santos RR, Soares MB, Zika virus infection induces mitosis abnormalities and apoptotic cell death of human neural progenitor cells. *Sci Rep* 6, 39775 (2016). [PubMed: 28008958]
60. Tang H, Hammack C, Ogden SC, Wen Z, Qian X, Li Y, Yao B, Shin J, Zhang F, Lee EM, Christian KM, Didier RA, Jin P, Song H, Ming GL, Zika Virus Infects Human Cortical Neural Progenitors and Attenuates Their Growth. *Cell Stem Cell* 18, 587–590 (2016). [PubMed: 26952870]
61. Vermillion MS, Lei J, Shabi Y, Baxter VK, Crilly NP, McLane M, Griffin DE, Pekosz A, Klein SL, Burd I, Intrauterine Zika virus infection of pregnant immunocompetent mice models transplacental transmission and adverse perinatal outcomes. *Nat Commun* 8, 14575 (2017). [PubMed: 28220786]
62. Driggers RW, Ho CY, Korhonen EM, Kuivanen S, Jaaskelainen AJ, Smura T, Rosenberg A, Hill DA, DeBiasi RL, Vezina G, Timofeev J, Rodriguez FJ, Levanov L, Razak J, Iyengar P, Hennenfent A, Kennedy R, Lanciotti R, du Plessis A, Vapalahti O, Zika Virus Infection with Prolonged Maternal Viremia and Fetal Brain Abnormalities. *N Engl J Med* 374, 2142–2151 (2016). [PubMed: 27028667]
63. Waldorf KMA, Nelson BR, Stencel-Baerenwald JE, Studholme C, Kapur RP, Armistead B, Walker CL, Merillat S, Vornhagen J, Tisoncik-Go J, Baldessari A, Coleman M, Dighe MK, Shaw DWW, Roby JA, Santana-Ufret V, Boldenow E, Li J, Gao X, Davis MA, Swanstrom JA, Jensen K, Widman DG, Baric RS, Medwid JT, Hanley KA, Ogle J, Gough GM, Lee W, English C, Durning WM, Thiel J, Gatenby C, Dewey EC, Fairgrieve MR, Hodge RD, Grant RF, Kuller L, Dobyns WB, Hevner RF, Gale M, Jr., Rajagopal L, Congenital Zika virus infection as a silent pathology with loss of neurogenic output in the fetal brain. *Nat Med*, (2018).
64. Aid M, Abbink P, Larocca RA, Boyd M, Nityanandam R, Nanayakkara O, Martinot AJ, Moseley ET, Blass E, Borducchi EN, Chandrashekar A, Brinkman AL, Molloy K, Jetton D, Tartaglia LJ, Liu J, Best K, Perelson AS, De La Barrera RA, Lewis MG, Barouch DH, Zika Virus Persistence in the Central Nervous System and Lymph Nodes of Rhesus Monkeys. *Cell* 169, 610–620 e614 (2017). [PubMed: 28457610]
65. Hirsch AJ, Smith JL, Haese NN, Broeckel RM, Parkins CJ, Kreklywich C, DeFilippis VR, Denton M, Smith PP, Messer WB, Colgin LM, Ducore RM, Grigsby PL, Hennebold JD, Swanson T, Legasse AW, Axthelm MK, MacAllister R, Wiley CA, Nelson JA, Streblow DN, Zika Virus infection of rhesus macaques leads to viral persistence in multiple tissues. *PLoS Pathog* 13, e1006219 (2017). [PubMed: 28278237]
66. Besnard M, Eyrolle-Guignot D, Guillemette-Artur P, Lastere S, Bost-Bezeaud F, Marcelis L, Abadie V, Garel C, Moutard ML, Jouannic JM, Rozenberg F, Leparac-Goffart I, Mallet HP, Congenital cerebral malformations and dysfunction in fetuses and newborns following the 2013 to 2014 Zika virus epidemic in French Polynesia. *Euro Surveill* 21, (2016).
67. Hazin AN, Poretti A, Turchi Martelli CM, Huisman TA, Microcephaly Epidemic Research G, Di D Cavalcanti Souza Cruz, M. Tenorio, A. van der Linden, L. J. Pena, C. Brito, L. H. Gil, D. de Barros Miranda-Filho, E. T. Marques, J. G. Alves, Computed Tomographic Findings in Microcephaly Associated with Zika Virus. *N Engl J Med* 374, 2193–2195 (2016).
68. Gottlieb DH, Capitanio JP, Latent variables affecting behavioral response to the human intruder test in infant rhesus macaques (*Macaca mulatta*). *Am J Primatol* 75, 314–323 (2013). [PubMed: 23229557]
69. Karere GM, Kinnally EL, Sanchez JN, Famula TR, Lyons LA, Capitanio JP, What is an "adverse" environment? Interactions of rearing experiences and MAOA genotype in rhesus monkeys. *Biol Psychiatry* 65, 770–777 (2009). [PubMed: 19103441]

70. Murray EA, Wise SP, Interactions between orbital prefrontal cortex and amygdala: advanced cognition, learned responses and instinctive behaviors. *Curr Opin Neurobiol* 20, 212–220 (2010). [PubMed: 20181474]
71. Bliss-Moreau E, Moadab G, Santistevan A, Amaral DG, The effects of neonatal amygdala or hippocampus lesions on adult social behavior. *Behav Brain Res* 322, 123–137 (2017). [PubMed: 28017854]
72. Moadab G, Bliss-Moreau E, Amaral DG, Adult social behavior with familiar partners following neonatal amygdala or hippocampus damage. *Behav Neurosci* 129, 339–350 (2015). [PubMed: 26030432]
73. Moadab G, Bliss-Moreau E, Bauman MD, Amaral DG, Early amygdala or hippocampus damage influences adolescent female social behavior during group formation. *Behav Neurosci* 131, 68–82 (2017). [PubMed: 28054806]
74. Brown MW, Aggleton JP, Recognition memory: what are the roles of the perirhinal cortex and hippocampus? *Nat Rev Neurosci* 2, 51–61 (2001). [PubMed: 11253359]
75. Zeamer A, Heuer E, Bachevalier J, Developmental trajectory of object recognition memory in infant rhesus macaques with and without neonatal hippocampal lesions. *J Neurosci* 30, 9157–9165 (2010). [PubMed: 20610749]
76. Raper J, Alvarado MC, Murphy KL, Baxter MG, Multiple Anesthetic Exposure in Infant Monkeys Alters Emotional Reactivity to an Acute Stressor. *Anesthesiology* 123, 1084–1092 (2015). [PubMed: 26313293]
77. Nguyen SM, Antony KM, Dudley DM, Kohn S, Simmons HA, Wolfe B, Salamat MS, Teixeira LBC, Wiepz GJ, Thoong TH, Aliota MT, Weiler AM, Barry GL, Weisgrau KL, Vosler LJ, Mohns MS, Breitbach ME, Stewart LM, Rasheed MN, Newman CM, Graham ME, Wieben OE, Turski PA, Johnson KM, Post J, Hayes JM, Schultz-Darken N, Schotzko ML, Eudailey JA, Permar SR, Rakasz EG, Mohr EL, Capuano S, 3rd, Tarantal AF, Osorio JE, O'Connor SL, Friedrich TC, O'Connor DH, Golos TG, Highly efficient maternal-fetal Zika virus transmission in pregnant rhesus macaques. *PLoS Pathog* 13, e1006378 (2017). [PubMed: 28542585]
78. Zare Mehrjardi M, Poretti A, Huisman TA, Werner H, Keshavarz E, Araujo Junior E, Neuroimaging findings of congenital Zika virus infection: a pictorial essay. *Jpn J Radiol* 35, 89–94 (2017). [PubMed: 28074379]
79. Zare Mehrjardi M, Carteaux G, Poretti A, Sanei Taheri M, Bermudez S, Werner H, Hygino da Cruz LC, Jr., Neuroimaging findings of postnatally acquired Zika virus infection: a pictorial essay. *Jpn J Radiol* 35, 341–349 (2017). [PubMed: 28447317]
80. <https://www.nih.gov/news-events/news-releases/study-examine-effects-zika-infection-guatemalan-infants-children>. (6 19, 2017).
81. Lanciotti RS, Lambert AJ, Holodniy M, Saavedra S, Signor Ldel C, Phylogeny of Zika Virus in Western Hemisphere, 2015. *Emerg Infect Dis* 22, 933–935 (2016). [PubMed: 27088323]
82. Hutchison RM, Womelsdorf T, Gati JS, Everling S, Menon RS, Resting-state networks show dynamic functional connectivity in awake humans and anesthetized macaques. *Hum Brain Mapp* 34, 2154–2177 (2013). [PubMed: 22438275]
83. Li CX, Patel S, Auerbach EJ, Zhang X, Dose-dependent effect of isoflurane on regional cerebral blood flow in anesthetized macaque monkeys. *Neurosci Lett* 541, 58–62 (2013). [PubMed: 23428509]
84. Tang CY, Ramani R, fMRI and Anesthesia. *Int Anesthesiol Clin* 54, 129–142 (2016). [PubMed: 26655513]
85. Vincent JL, Patel GH, Fox MD, Snyder AZ, Baker JT, Van Essen DC, Zempel JM, Snyder LH, Corbetta M, Raichle ME, Intrinsic functional architecture in the anaesthetized monkey brain. *Nature* 447, 83–86 (2007). [PubMed: 17476267]
86. Beauregard M, Bachevalier J, Neonatal insult to the hippocampal region and schizophrenia: a review and a putative animal model. *Can J Psychiatry* 41, 446–456 (1996). [PubMed: 8884034]
87. Wang J, Vachet C, Rumpel A, Gouttard S, Ouziel C, Perrot E, Du G, Huang X, Gerig G, Styner M, Multi-atlas segmentation of subcortical brain structures via the AutoSeg software pipeline. *Front Neuroinform* 8, 7 (2014). [PubMed: 24567717]

88. Knickmeyer RC, Styner M, Short SJ, Lubach GR, Kang C, Hamer R, Coe CL, Gilmore JH, Maturational trajectories of cortical brain development through the pubertal transition: unique species and sex differences in the monkey revealed through structural magnetic resonance imaging. *Cereb Cortex* 20, 1053–1063 (2010). [PubMed: 19703936]
89. Andersson JL, Skare S, Ashburner J, How to correct susceptibility distortions in spin-echo echo-planar images: application to diffusion tensor imaging. *Neuroimage* 20, 870–888 (2003). [PubMed: 14568458]
90. Gorgolewski K, Burns CD, Madison C, Clark D, Halchenko YO, Waskom ML, Ghosh SS, Nipype: a flexible, lightweight and extensible neuroimaging data processing framework in python. *Front Neuroinform* 5, 13 (2011). [PubMed: 21897815]
91. Fair DA, Cohen AL, Power JD, Dosenbach NU, Church JA, Miezin FM, Schlaggar BL, Petersen SE, Functional brain networks develop from a "local to distributed" organization. *PLoS Comput Biol* 5, e1000381 (2009). [PubMed: 19412534]
92. Fair DA, Dosenbach NUF, Church JA, Cohen AL, Brahmbhatt S, Miezin FM, Barch DM, Raichle ME, Petersen SE, Schlaggar BL, Development of distinct control networks through segregation and integration. *P Natl Acad Sci USA* 104, 13507–13512 (2007).
93. Fair DA, Nigg JT, Iyer S, Bathula D, Mills KL, Dosenbach NU, Schlaggar BL, Mennes M, Gutman D, Bangaru S, Buitelaar JK, Dickstein DP, Di Martino A, Kennedy DN, Kelly C, Luna B, Schweitzer JB, Velanova K, Wang YF, Mostofsky S, Castellanos FX, Milham MP, Distinct neural signatures detected for ADHD subtypes after controlling for micro-movements in resting state functional connectivity MRI data. *Front Syst Neurosci* 6, 80 (2012). [PubMed: 23382713]
94. Iyer SP, Shafraan I, Grayson D, Gates K, Nigg JT, Fair DA, Inferring functional connectivity in MRI using Bayesian network structure learning with a modified PC algorithm. *Neuroimage* 75, 165–175 (2013). [PubMed: 23501054]
95. Miranda-Dominguez O, Mills BD, Grayson D, Woodall A, Grant KA, Kroenke CD, Fair DA, Bridging the gap between the human and macaque connectome: a quantitative comparison of global interspecies structure-function relationships and network topology. *J Neurosci* 34, 5552–5563 (2014). [PubMed: 24741045]
96. McLaren DG, Kosmatka KJ, Kastman EK, Bendlin BB, Johnson SC, Rhesus macaque brain morphometry: a methodological comparison of voxel-wise approaches. *Methods* 50, 157–165 (2010). [PubMed: 19883763]
97. McLaren DG, Kosmatka KJ, Oakes TR, Kroenke CD, Kohama SG, Matochik JA, Ingram DK, Johnson SC, A population-average MRI-based atlas collection of the rhesus macaque. *Neuroimage* 45, 52–59 (2009). [PubMed: 19059346]
98. Power JD, Barnes KA, Snyder AZ, Schlaggar BL, Petersen SE, Spurious but systematic correlations in functional connectivity MRI networks arise from subject motion. *Neuroimage* 59, 2142–2154 (2012). [PubMed: 22019881]
99. Power JD, Mitra A, Laumann TO, Snyder AZ, Schlaggar BL, Petersen SE, Methods to detect, characterize, and remove motion artifact in resting state fMRI. *Neuroimage* 84, 320–341 (2014). [PubMed: 23994314]
100. Styner M, Knickmeyer R, Joshi S, Coe C, Short SJ, Gilmore J, Automatic brain segmentation in rhesus monkeys. *P Soc Photo-Opt Ins* 6512, L5122–L5122 (2007).
101. Paxinos G, Huang X, Toga AW, *The Rhesus Monkey Brain in Stereotaxic Coordinates*. (Academic Press, San Diego, CA, 1999).
102. Saleem KS, Logothetis NK, *A Combined MRI and Histology Atlas of the Rhesus Monkey Brain in Stereotaxic Coordinates*. (Academic Press, San Diego, CA, ed. 2nd edition, 2012).
103. Payne C, Bachevalier J, Crossmodal integration of conspecific vocalizations in rhesus macaques. *PLoS One* 8, e81825 (2013). [PubMed: 24236218]

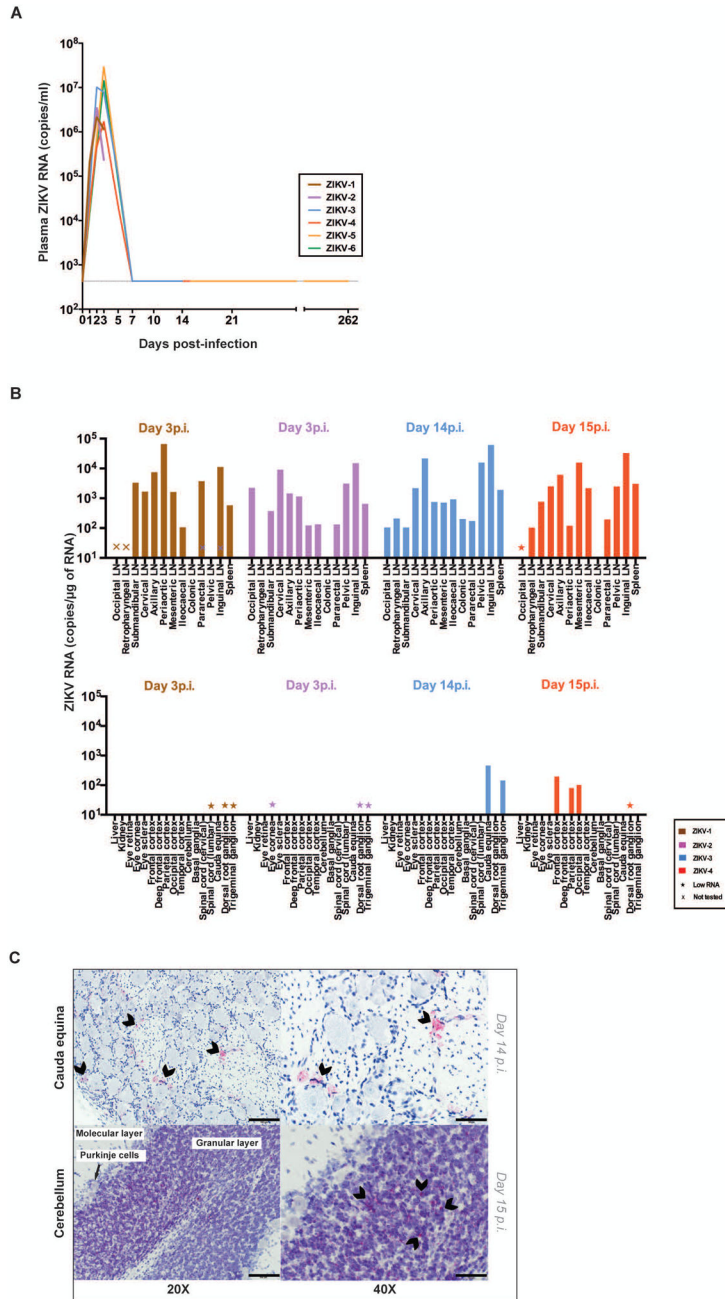


Figure 1. ZIKV RNA in blood and tissues.

(A) Plasma ZIKV RNA concentration as measured by RT-PCR. (B) Assessment of ZIKV RNA concentration by RT-PCR in lymphoid (top) and non-lymphoid tissues (bottom) at day 3 or 14-15 post-infection. Low RNA indicates < 20 ng/μl was run in the PCR. (C) Representative detection of ZIKV RNA by RNAscope *in situ* hybridization in nervous system tissues. Arrowheads indicate some of the most intense RNAscope signals (red). No arrowheads were placed on the bottom left panel as the RNAscope signal was diffusely positive in the cerebellum at this magnification. The scale bars represent 100μm and 50μm in the left and right panels, respectively. 4-5 images per brain area were examined.

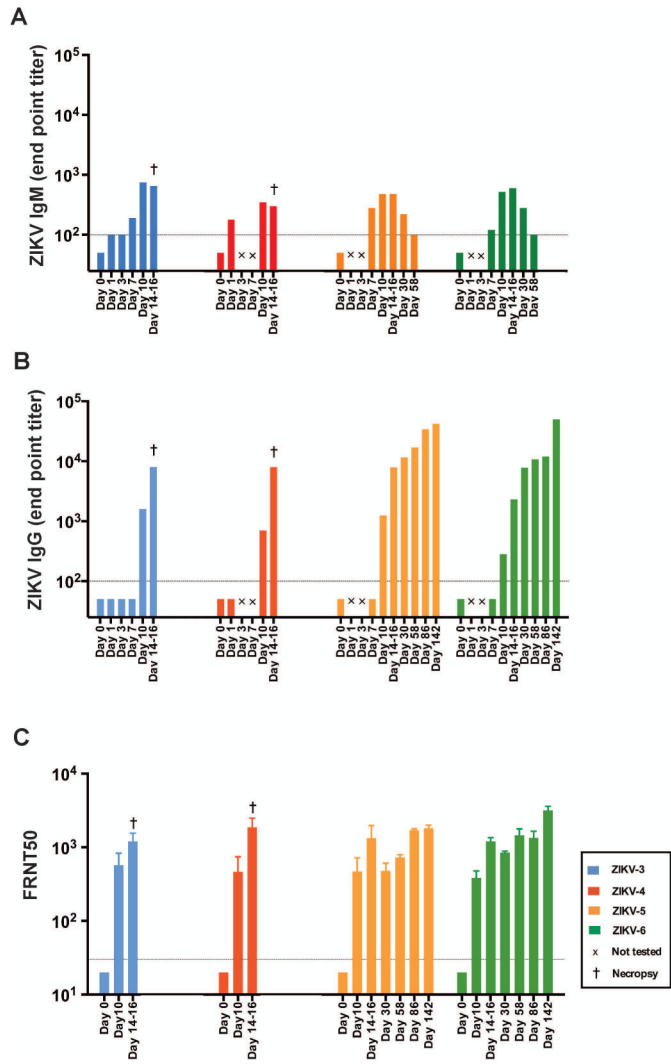


Figure 2. Humoral immune response to ZIKV-infection. (A) ZIKV E-specific IgM plasma concentrations measured by ELISA. (B) ZIKV E-specific IgG plasma concentrations measured by ELISA. (C) ZIKV neutralization activity of RM plasma measured by focus reduction neutralization test (FRNT). The dashed line indicates the limit of detection for the respective assays (i.e., the lowest dilution tested). Undetectable values were set at half the lower limit of detection for visualization purposes.

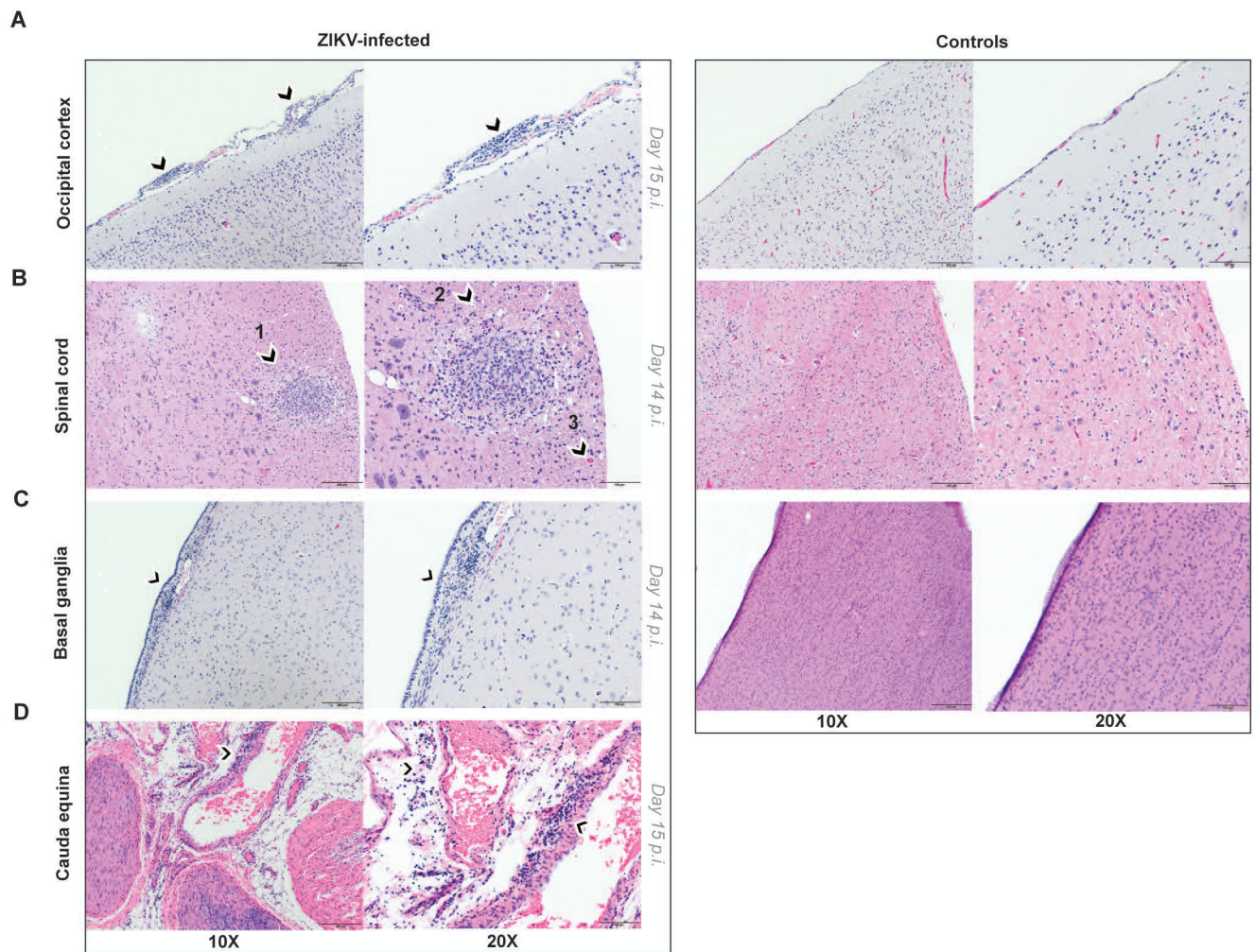


Figure 3. Neurohistopathology of postnatal ZIKV infection in infant RMs.

Hematoxylin and eosin (H&E) staining of nervous tissue sections from ZIKV-infected infant RM (left) and age-matched controls (right). **(A)** Occipital cortex with multifocal meningeal infiltrates (arrowheads) in ZIKV-infected RM. **(B)** Anterior thoracic spinal cord with circumscribed inflammatory focus (arrowhead 1), dilated axons (arrowhead 2) and spheroid formation (arrowhead 3) in ZIKV-infected RM. **(C)** Basal ganglia showing hypercellularity with glial cells in the underlying stroma of the ependymal epithelial cell lining (arrowhead) in ZIKV-infected RM. **(D)** cauda equina with multifocal perivascular inflammatory cells (arrowheads) in ZIKV-infected RM. Scale bars, 200 μ m (10X), 100 μ m (20X). 4-5 images per brain area were examined.

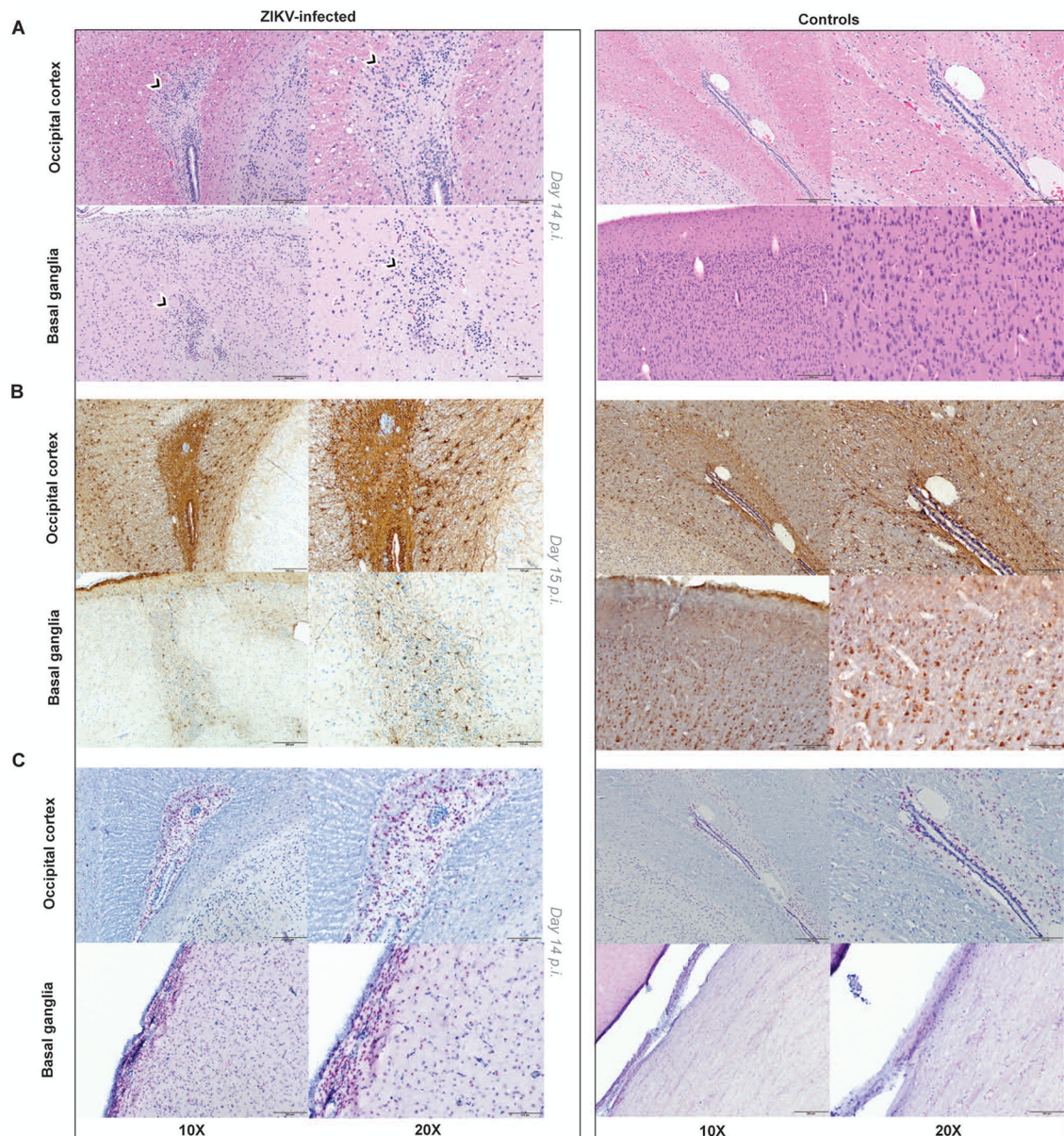


Figure 4. Astrogliosis and apoptosis of brain regions in postnatally-infected infant RMs. Staining of central nervous system tissue sections from ZIKV-infected infant RM (left) and age-matched controls (right). **(A)** H&E staining with moderate astrogliosis in the white matter in the periventricular region of the occipital cortex and glial nodule in the grey matter of the basal ganglia in ZIKV-infected RM. **(B)** GFAP (Glial Fibrillary Acidic Protein) staining of the occipital cortex and basal ganglia demonstrating reactive astrocytes in ZIKV-infected RM. **(C)** Caspase-3 staining of the occipital cortex and basal ganglia demonstrating increased apoptosis in ZIKV-infected RM. Scale bars, 200 μ m (10X), 100 μ m (20X). 4-5 images per brain area were examined.

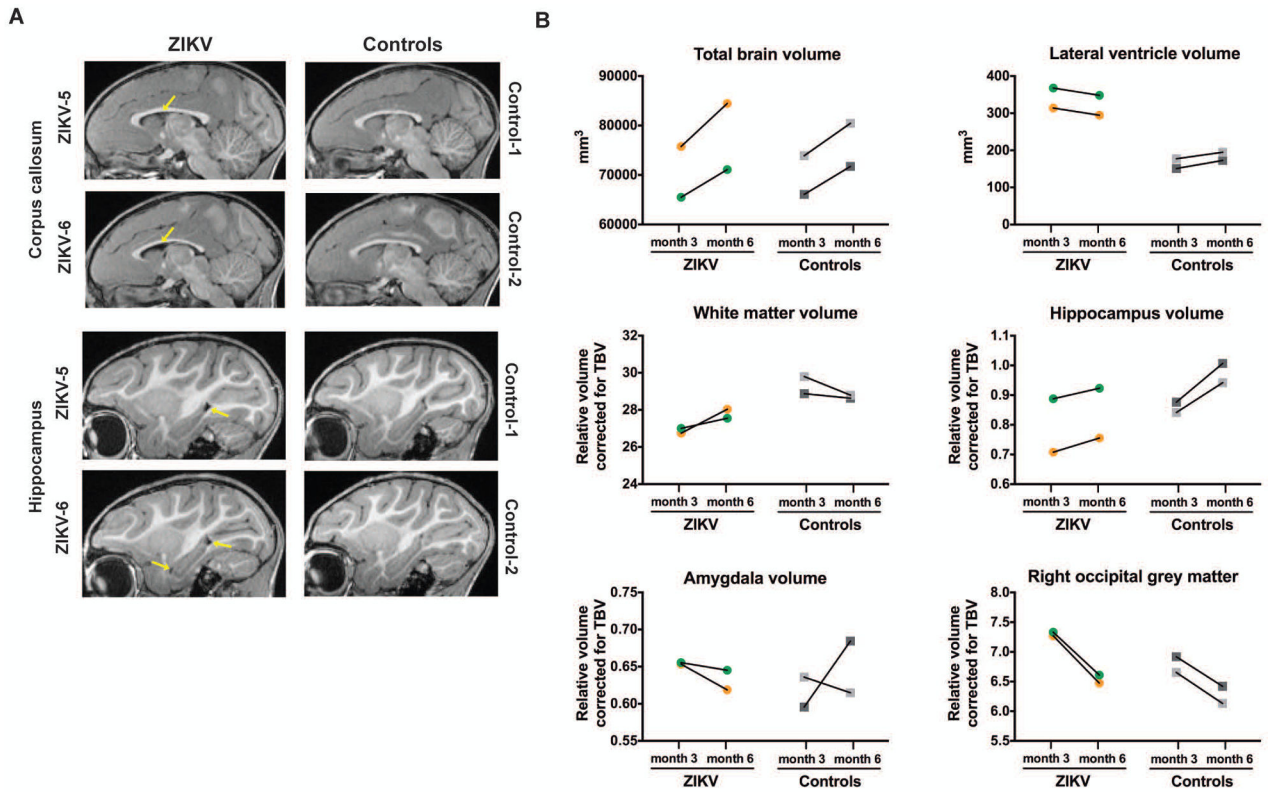


Figure 5. Structural neuroimaging at three and six months of age after postnatal ZIKV infection of infant RMs.

(A) Sagittal T1-weighted structural MRI images through the corpus callosum (top) and hippocampus (bottom) at six months of age; yellow arrows illustrate the increased lateral ventricle volume in ZIKV-infected RMs. (B) Structural MRI measurements in cubic millimeters for total brain volume and lateral ventricle volume as well as specific grey and white matter areas corrected for total brain volume (TBV) at three and six months of age in ZIKV-infected RMs and controls. The correction used was specific brain region/TBV x 100.

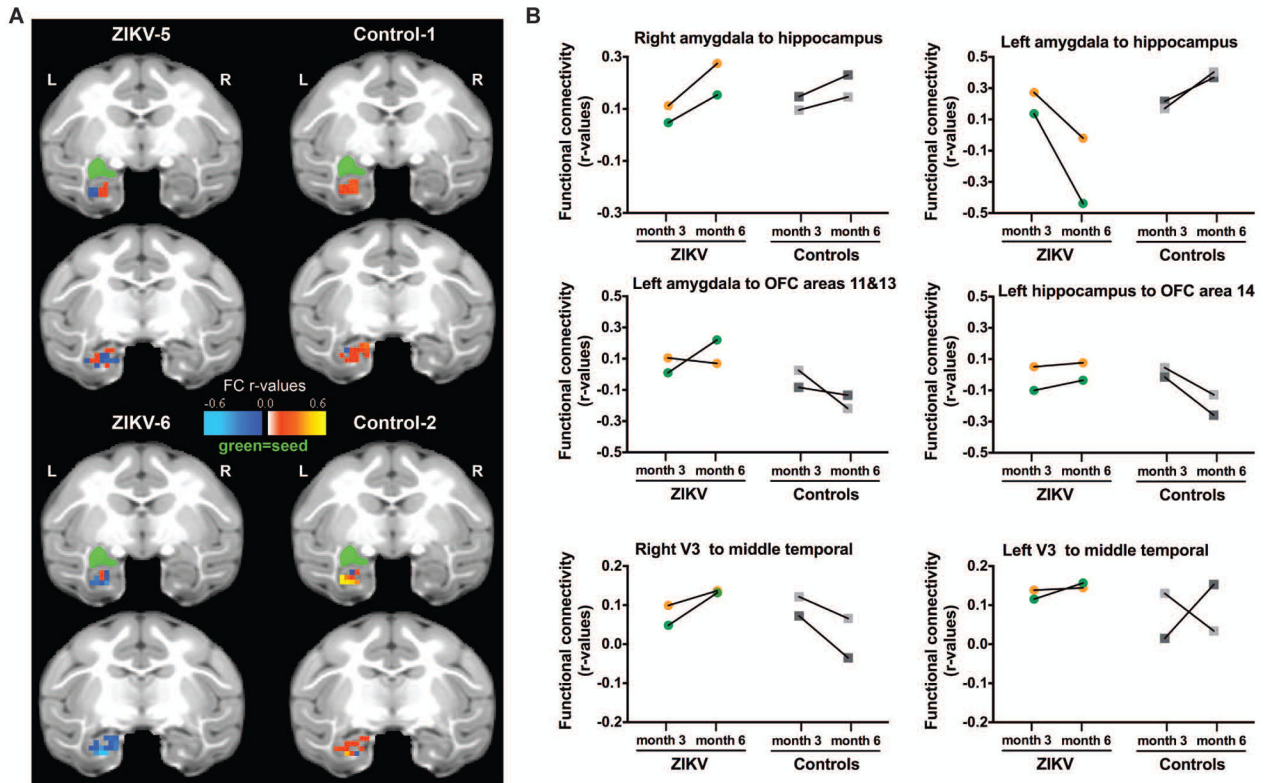


Figure 6. Functional neuroimaging at three and six months of age after postnatal ZIKV infection of infant RMs.

(A) Depiction of Amygdala-Hippocampus resting state functional connectivity (FC) measured by rs-fMRI at six months of age displayed in the UNC-Emory RM infant atlas (35). Images show the same two coronal slice series in each subject with the seed (green) placed in the left amygdala and the FC r-values in the hippocampus colored according to the scale provided. Results for the right amygdala seed not shown for clarity, but are provided in Table S4. L=left hemisphere; R=right hemisphere; r-values=raw FC correlations. (B) rs-fMRI longitudinal measurements of FC between specific regions of interest at three and six months of age in ZIKV-infected RM and controls. V3 = visual area 3; OFC = orbital frontal cortex.

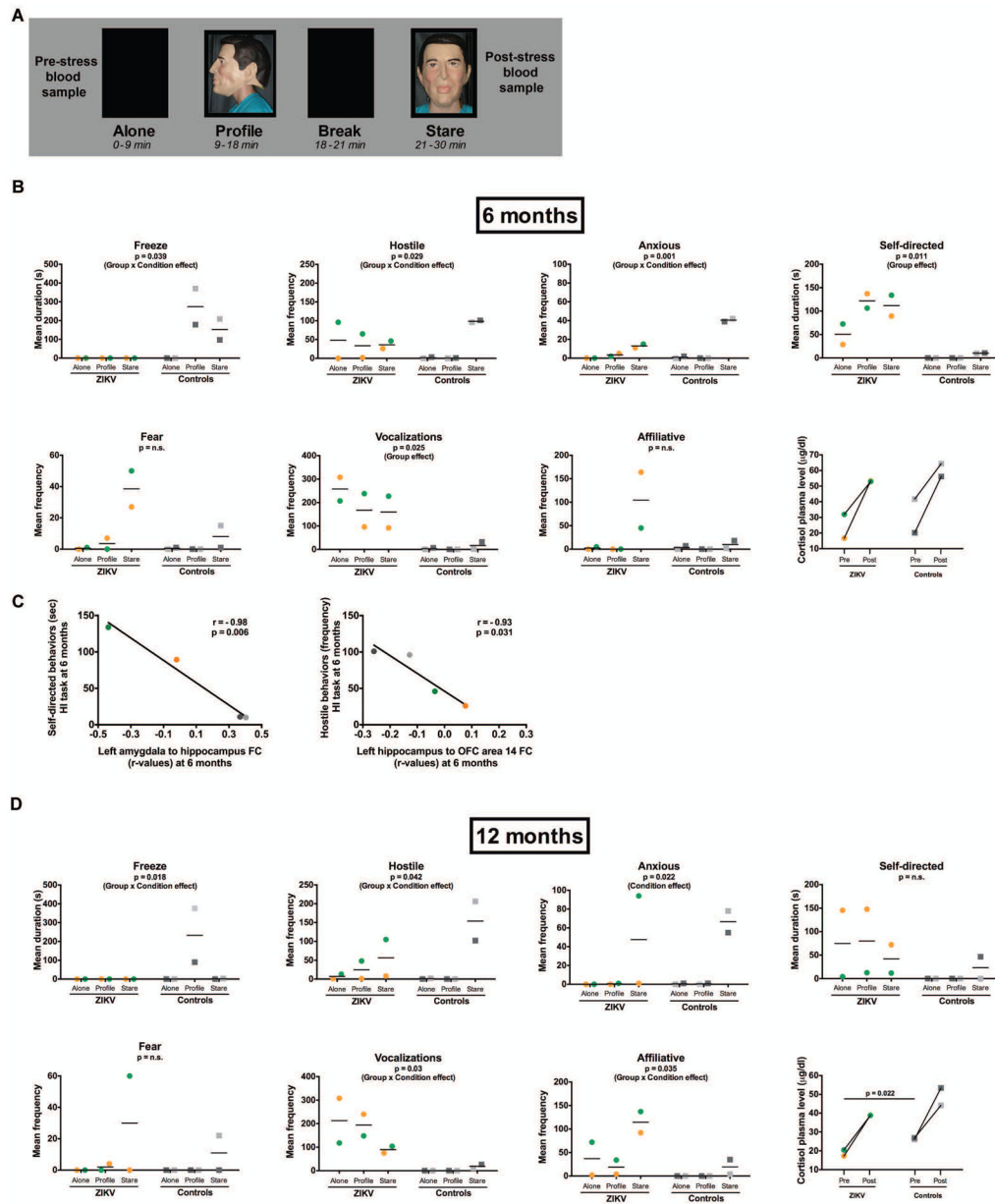


Figure 7. Assessment of the behavioral response to acute stress using the Human Intruder Paradigm at six and twelve months of age after postnatal ZIKV infection of infant RMs. (A) Description of the Human Intruder task measuring the ability to modulate emotional behavior based on the salience of the threat presented. ALONE: the animal is placed alone in a novel room; PROFILE: a human intruder wearing a mask presents his profile to the animal; STARE: the intruder makes direct eye contact with the animal. (B) Comparison of behaviors using a standard ethogram (described in Table S5) in response to the three stress levels in ZIKV-infected infant RMs and age-matched uninfected controls at six months of age. Bottom right graph shows and pre- and post-stress plasma cortisol concentrations. (C) Correlations between the observed behavioral responses to stress with functional connectivity (r-values) between specific brain regions of interest in ZIKV-infected infant RMs and age-matched uninfected controls at six months of age. (D) Comparison of

behaviors using a standard ethogram (described in Table S5) in response to the three stress levels in ZIKV-infected infant RMs and age-matched uninfected controls at twelve months of age. Bottom right graph shows pre- and post-stress plasma cortisol concentration.

Author Manuscript

Author Manuscript

Author Manuscript

Author Manuscript